NPL Report CMAM 64

Interim report on the fabrication and characterisation of the surface of silicon artefacts used in the Avogadro project

S P Downes

April 2001

Interim report on the fabrication and characterisation of the surface of silicon artefacts used in the Avogadro project

S P Downes
National Physical Laboratory
Teddington, Middlesex, United Kingdom, TW11 0LW

April 2001

ABSTRACT

A new definition of the kilogram is being sought. A possibility is to relate the kilogram to an atomic mass, through the accurate measurement of the Avogadro constant. This approach is realised through spheres manufactured from extremely pure, single crystal silicon. One parameter to be determined is the bulk density of the silicon crystal. However, the measured density will include a contribution due to the surface oxide and any contaminants that are adsorbed onto a sphere's surface. Furthermore, the scale and structure of damage in the near surface region of the crystal (arising from the manufacturing process) may also significantly change the measured density.

NPL has a project to manufacture and characterise the surface of such artefacts. Three complementary techniques, namely Variable Angle Spectroscopic Ellipsometry (VASE), Rutherford Backscattering Spectroscopy (RBS) and X-ray Photoelectron Spectroscopy (XPS), are being used to determine the structure, composition and thickness of surface layers. Atomic Force Microscopy (AFM) is used to determine the morphology of the surface and to monitor the effective removal of surface contaminants arising from the manufacturing stages.

Large discrepancies have been found when determining oxide thickness using VASE, RBS and XPS. However, these values are also strongly correlated. Damage to the crystal structure has been identified and quantified using RBS. The scale of the damage suggests an amorphised region with a depth of up to 50 Angstroms. The presence of a carbonaceous overlayer has been detected using XPS. The work reported here describes the current state of this project and future experimental stages.

ISSN N^{o} 1369-6785

National Physical Laboratory
Teddington, Middlesex, United Kingdom, TW11 0LW

Approved on behalf of the Managing Director, NPL,
by Dr Graham Torr, Head,
Centre for Mechanical and Acoustical Metrology

CONTENTS

1 BACKGROUND

A new definition of the kilogram is being sought. A possibility is to relate the kilogram to an atomic mass, through the accurate measurement of the Avogadro constant. This approach is realised through spheres manufactured from extremely pure, single crystal silicon. The work described in this report forms part of a larger study to characterise the surface of silicon artefacts that are fabricated by a mechanical polishing process. This document describes the polishing processes used at NPL and the techniques being developed to characterise the surface. The surface measurements are being made with the facilities and expertise available at the University of Surrey. Section §5 of this report contains detail of the analysis of these measurements to date. Future experimental stages are outlined in §6. Publication of this report represents the completion of milestone 1.3.2.1 of the NMS Programme for Mass Metrology October 1999 - September 2002.

1.1 International Avogadro project to re-define the kilogram

The Avogadro approach to re-defining the kilogram is based on the determination of an atomic mass with sufficient accuracy to make possible a new definition of the kilogram. The first stage of this work requires an accurate measurement of the *Avogadro constant* N_A. The background to this approach, together with the participating National Measurement Institutions NMI's and their areas of research, is described in the NPL Report CMAM 11 [1].

1.2 Studies of silicon artefacts at NPL

Single crystal silicon spheres are used to realise the Avogadro approach. One of the parameters to be determined is the bulk density of the silicon crystal. The bulk density is measured directly from a sphere's mass and volume. However, the polishing stages during manufacture (§2) involve an abrasive process to remove material. Based on related studies [2], it is speculated that polishing causes physical damage to the crystalline structure near the surface as well as influencing the growth of the surface oxide (§3). Any departure from a perfect single crystal will require a correction to the measured bulk density [3]. This is also

true of the native oxide that forms after polishing and any contaminants that are adsorbed on a sphere's surface (§3.1). To make the necessary corrections to the measured density one needs to determine the thickness of these damaged, oxide and adsorbed layers (§3.2)with a combined uncertainty of just a few Ångstroms (10^{-10} m). This uncertainty is also required to minimise corrections when determining the diameter of spheres interferometrically [4].

The physical and chemical interaction between the surface and the surrounding environment will determine the long-term mass stability of these artefacts. In parallel with the work described in this report, the mass stability of silicon artefacts is being investigated.

1.3 Scientific objectives

Avogadro work at NPL can be grouped under the categories of *mass related* and *surface characterisation.* The scientific objectives in these two areas are stated below. The work reported here describes the progress made toward the surface characterisation of silicon artefacts.

1.3.1 Mass related

- develop necessary techniques to fabricate/polish cylindrical silicon artefacts for mass stability investigations
- determine mass stability of silicon artefacts in ambient conditions
- quantify mass change due to adsorption/de-sorption of water over a range of humidities
- determine mass stability of silicon artefacts in a vacuum
- quantify mass change due to adsorption/de-sorption of contaminants due to ambient/vacuum cycling

1.3.2 Surface characterisation

- develop necessary techniques to fabricate/polish flat and spherical silicon artefacts

- develop complementary surface analysis techniques to determine the thickness, structure and composition of surface contaminating layers (§3.1) on polished flat silicon surfaces. Investigate correlation for different crystallographic orientations
- establish Variable Angle Spectroscopic Ellipsometry (VASE) as a stand-alone technique for the measurement of the thickness of contaminating layers on polished silicon surfaces
- characterisation of the surface of polished silicon spheres. Investigate correlation with crystallographic orientation
- growth of a stoichiometric, thermal oxide (§3.1.2) on a sphere's surface

2 SILICON ARTEFACTS

2.1 Fabrication of silicon artefacts at NPL

Three distinct geometries of artefact are being manufactured for this project: spherical, cylindrical and flat. An objective of this work (§1.3) is to develop a fabrication process at NPL for the production of silicon spheres with a well-defined surface (§2.2 and §3.1) and a mass that has been closely controlled to 1 kg. Cylindrical artefacts have been manufactured to investigate the mass stability of silicon. A range of flat surfaces have been polished to aid in the development of the analytical techniques (§4) being used to characterise the surface. These include different crystallographic orientations (§5.2) to investigate any correlation with contamination layers.

2.2 Surface topography

The Avogadro approach to re-defining the kilogram is being realised through the characterisation of spherical artefacts manufactured from silicon single crystal. These artefacts have a nominal mass[1] of 1 kg and a diameter of approximately 93 mm. A requirement of this approach is to determine the average diameter of these artefacts with an uncertainty of just a few Ångstroms. As a consequence, their sphericity must be tightly controlled [5] and their surface roughness kept to a minimum. Controlling the form of the spheres is not a goal of the work reported here. However, producing the best achievable surface finish is. The surface characteristics will also affect the mass stability of these artefacts. In practical terms, the roughness must be controlled to a few Ångstroms or less. Essential to developing the polishing process, be it for spheres, cylinders or flats, is the feedback gained from the measurement of surface topography using an Atomic Force Microscope (§4.5).

[1] The mass should be adjusted to 1 kg ± 10 mg to minimise any scale errors associated with the mass comparators used to weigh the silicon artefacts.

2.3 Fabrication stages

The manufacturing and polishing stages have all been developed in-house using the expertise and facilities of the NPL Optical Workshop. All three types of artefact share similar manufacturing stages and are based on those traditional to precision optical polishing and grinding. These stages can be summarised as:

- Shaping the artefact from a cylindrical ingot using machine tools equipped with diamond tooling
- Smoothing with aluminium oxide loose abrasives
- Polishing with a colloidal suspension of very fine particles (aluminium oxide or silica)

Vital to all stages is the removal of sufficient material to ensure that any damage to the lattice structure (sub-surface damage) resulting from the previous stage has been removed. Typically, the depth of material removed is three to four times that of the proceeding grit size. This process should ensure that any damage to the lattice is due only to the final stage of polishing.

2.3.1 Flats

The polishing procedure for flat surfaces was the first to be established. Samples were taken from a cylindrical boule, cut nominally along a (100) crystallographic plane. The misalignment of the cut is not known. The smoothing and polishing stages were very similar to those used for high quality optical components. Following the initial cut, using a resin-bonded diamond-grinding wheel, the artefacts were smoothed using aluminium oxide loose abrasives with average grit sizes of 20 and 10 μm respectively. Smoothing is purely a manual process, each stage taking several hours to remove all the damage arising from the previous stage.

Polishing was achieved on a resin based lapping machine, using an optical polishing slurry consisting of a colloidal suspension of aluminium oxide with a particulate size of around

1 μm. In practice, the particles will break down during use, which is the underlying reason why a surface roughness on a nanometre scale can be achieved. This last stage can take up to 30 hours of polishing to remove all damage from the previous smoothing stage. Great care has to be taken to keep particulate contaminants away from the lap as sleeks on the surface are very easily introduced.

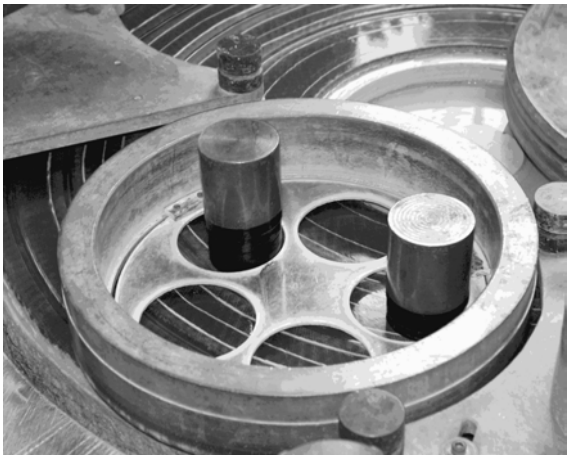

Figure 2–1. Two artefacts being polished on a lapping machine in the NPL Optical Workshop

Figure 2–1 shows two flat surfaces undergoing their final polish on the lap. Weights are added to the top of each artefact (in this case, a brass cylinder) to ensure that a consistent contact pressure is maintained throughout the process. Crucial to both smoothing and polishing stages alike, is the movement of the artefact with respect to the abrasive medium. This must be with a random motion to ensure there is no bias to the material removal process that might otherwise cause surface features to be present on the finished artefact. The Roughness average[2] Ra (excluding areas where surface contaminants were identified) was measured as being between 0.2 and 0.3 nm (§5.9.1).

[2] Roughness average (or the arithmetic mean deviation of roughness profile) Ra is defined as the arithmetic mean of the absolute values of the departures of the profile from the mean line.

2.3.2 Cylinders

All artefacts were taken from a cylindrical boule supplied by Wacker-Chemitronic[3]. This boule was grown with its axis along a <100> direction. A trepanner with a diamond cutting edge was used to rough out an oversized cylinder. The top and bottom face of this cylinder were then polished using the process described at (§2.3.1). However, polishing the side of the cylinder proved much more problematic due to the non-random nature of the polishing action.

The only practical means of polishing a cylinder's side is to mount the artefact on a lathe. Smoothing and polishing is achieved by the use of a suitably shaped tool which is manually worked along the length of the artefact. The tool for the smoothing stages consisted of an aluminium strip that was shaped into a right-angle, providing two points of contact with the artefact. The first stage was to remove damage arising from the trepanner using silicon carbide loose abrasives with a grit size of around 50 μm. Smoothing then proceeded using aluminium oxide loose abrasives with grit sizes of 20 and 10 μm respectively. However, at smaller grit sizes, contact between the tool's surface and the artefact is unavoidable and small cuts appear on the surface. The right-angle tool was abandoned at this stage and, instead, a strip of aluminium was formed to roughly take up the radius of the cylinder. Several different combinations of polisher matrix and slurry were tried. The most effective combination (i.e. least likely to cause damage) proved to be a matrix of expanded Polyurethane foam (which was cemented to the inner surface of the strip) with a colloidal suspension of aluminium oxide, followed by one of silica for the final polish.

Examination of the finished surface with an atomic force microscope (§5.9.3) has revealed a series of grooves which clearly relate to the non-random nature of the polishing action. However, the surface roughness was measured as 0.5 nm. One can surmise that the underlying surface would have a lower value.

[3] Wacker-Chemitronic GmbH, D-84479 Burghausen, Germany

2.3.3 Sphere

An experimental silicon sphere has now been manufactured, the stages of which are demonstrated by Figure 2–2. The starting point for manufacturing a sphere is to create a cube. The diameter of the cylindrical boule, however, was too small to allow a cube with an edge length of 95 mm to be machined from its bulk. Hence, the cylindrical boule was cemented into a jig, manufactured from Crown glass, as shown. A milling machine, with a diamond edged cutting tool, was then used to systematically remove all edges and corners. This process is continued until the artefact was reduced to a polyhedron having 18 facets. The next stage was to grind away these facets leaving a sphere. Two tools were fashioned for this purpose. They were manufactured from an aluminium tube (with an approximate wall thickness of 1 cm) and an internal diameter that was approximately 25% less than that of the sphere. An annulus was cut on one inside edge of each tool. A similar pair of tools were also used for the smoothing and polishing stages. As can be seen below, one tool is mounted vertically on a spindle connected to a motor which turns the spindle at approximately 60 rpm. The sphere is supported within the annulus of this tool. The other tool is manually held in contact with sphere and is worked with a random motion to ensure that the sphere is polished uniformly across its surface. Grinding was carried out using coarse silicon carbide abrasives with grit sizes of 600, 100 and 50 μm respectively.

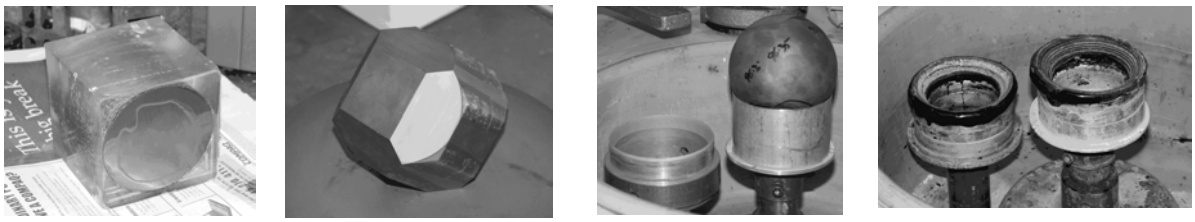

Figure 2–2. Sphere fabrication stages (left to right); cementing a cylindrical boule into a glass block; removing corners/edges with a milling machine; a sphere during the smoothing stage; and tool faces coated with an optical pitch for polishing

A pair of new tools were used for the final smoothing and polishing stages. Smoothing proceeded using aluminium oxide loose abrasives with grit sizes of 20 and 10 μm. To avoid contact between the tool and the artefact during polishing, the annulus of each tool was coated with a matrix of optical pitch. The polishing medium was a colloidal suspension of silica. This final polishing stage took around 20 hours to completely remove the damage from

the 10 μm smoothing stage. The next stage will be to use an AFM to determine the surface topography of this sphere (§6).

3 SURFACE CONTAMINANTS AND PHYSICAL MODEL

3.1 Contaminants

A goal of this work is the identification and characterisation of any contaminants that are present on the surface of silicon spheres. Here, the term contaminant is used to describe any material that is not silicon in its crystalline form. The following contaminants may be found on a silicon surface that has been mechanically polished.

3.1.1 Damage to the lattice structure

The removal of material through a physical polishing process will involve a variety of mechanisms that involve elastic and plastic deformation as well as fractures to the crystal lattice [6]. When the local density of plastic deformation is high the structure may become amorphous [7]. This type of damage may be significant. Both the physical density and optical properties of these regions will be different from that of silicon in its normal crystalline form, requiring corrections to the measured density and thickness of contaminating layers (§4.2) as determined by ellipsometry. Dislocations and point defects will decrease the density.

3.1.2 Oxidation

When exposed to ambient conditions a silicon surface will always oxidise to form silicon dioxide (SiO_2) [8]. After the formation of the first monolayer, the process is one of diffusion by oxygen atoms through the oxide until fresh silicon is reached. Thus, the oxide grows into the crystal. As the oxide gets thicker, so the diffusion process takes longer and the growth rate is slowed.

An oxide which forms under normal ambient conditions is referred to as a native oxide and has an amorphous structure. If the composition is SiO_2 then it is referred to as being

stoichiometric[4]. Non-stoichiometric oxides are possible depending on the environment at the time of formation. For instance, if water is present, then hydroxyl bonds may be formed as the oxide grows (giving SiO_XOH_Y where 2X+Y=4), thereby increasing the stoichiometry (i.e. increasing the ratio of oxygen relative to silicon). Typically, oxide layers grown by the semiconductor industry are produced in a dry oxygen environment, at high temperatures (800°C or greater) to increase the growth rate [9]. This process forms a well defined, stoichiometric layer and is referred to as a thermal oxide.

3.1.3 Adsorbed contaminants

Contaminants will be adsorbed onto the surface from a variety of sources. The manner of their bonding may be physisorbed (i.e. such as molecular water and hydrocarbons from the surrounding environment) or chemisorbed (i.e. such as hydroxyl groups and ionic species from the polishing media).

3.2 Surface model

The first stage in the analysis of this work has been to consider a simple ‘layered model’ to describe the presence of surface contaminants. The model is based on existing understanding of polished surfaces [7] and the concept of this approach is shown by Figure 3–1. A more complicated model (possibly including interfacial roughness) may need to be developed at a later stage as more is understood of the effects of polishing and oxide growth.

[4] A stoichiometric compound is one in which the ratio of the number of atoms to each other, as determined from the atomic weights, is a ratio of small whole numbers.

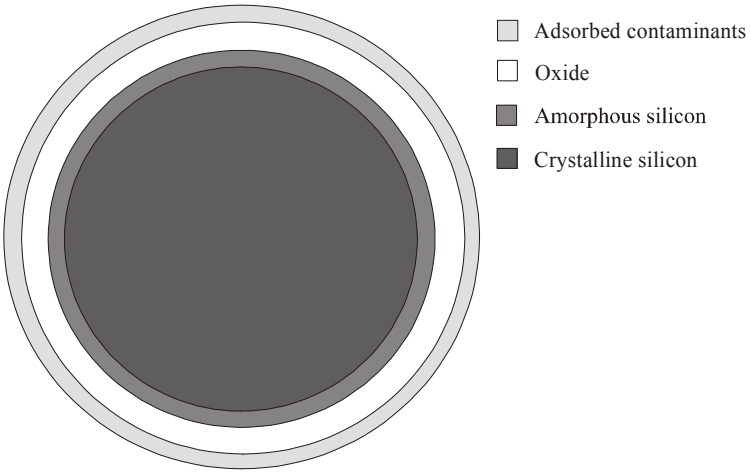

Figure 3–1. Layered approach to modelling contaminants on the surface of a silicon sphere

The density of any of these contaminating layers may be different from that of the bulk crystal. With the exception of damage to the silicon lattice, they may all affect an artefact's mass stability.

4 ANALYTICAL TECHNIQUES

4.1 Complementary methods

Preliminary measurements of the combined thickness of these contaminating layers suggest a value of the order of a few nanometres (§5.4). Unfortunately, there is no single analytical technique that can be used to identify and quantify all the contaminants described in §3. Furthermore, on this scale of measurement, most techniques involve a modelling process whereby certain assumptions are made regarding the properties of these extremely thin films (i.e. their optical constants, stoichiometry or density is assumed). Thus, it is necessary to use complementary techniques to fully characterise these types of structures. Table 4-1 lists the techniques that have been used in this study and the properties that can be measured by each technique.

Physical parameter	VASE	RBS	XPS	AFM
Surface topography				✓
Adsorbed contaminants	✓		✓	
Oxide thickness	✓	✓	✓	
Oxide stoichiometry			✓	
Amorphous thickness	✓	✓		
Where VASE is Variable Angle Spectroscopic Ellipsometry (§4.2) RBS is Rutherford Backscattering Spectroscopy (§4.3) XPS is X-ray Photoelectron Spectroscopy (§4.4) AFM is Atomic Force Microscopy (§4.5)				

Table 4-1. Physical parameters of thin films/contaminants measured by each technique

Of the techniques that can determine the thickness of these layers, Variable Angle Spectroscopic Ellipsometry (VASE) has the potential to measure all the contaminants involved with sub-monolayer sensitivity [10]. It is also the only technique that can be used in ambient conditions. As such, accommodation of a sphere is relatively straightforward. In contrast, both RBS and XPS operate under vacuum conditions and are generally not equipped with goniometer stages that can accommodate large samples such as 1 kg silicon spheres. However, measurement of the thickness of ultra-thin layers by ellipsometry is reliant on a knowledge of the optical constants of the layers (§4.2.2). An objective of this work is to

establish the use of VASE as a stand-alone technique for characterising the thickness of surface layers on Avogadro spheres, following determination of their optical constants.

4.2 Ellipsometry

4.2.1 Background

Ellipsometry can be used to determine the optical constants (the real n and imaginary k components of the complex refractive index) of a sample being studied. It is well suited to the characterisation of thin films on an optically well-defined substrate. If the optical constants of a film are known (or have been assumed), its thickness may be calculated. In this work, ellipsometry has been used to determine the thickness of oxide layers and amorphous silicon layers where they are present. It is hoped to extend the use of this method to be able to identify and measure the thickness of contaminants that are adsorbed on the surface (§6.2). For thick films, the technique can reliably determine both the optical constants and thickness, but in films less than approximately 20 nm there is correlation between the parameters.

4.2.2 Principle of ellipsometry

Ellipsometry measures the change in the polarisation state of a light beam that has been reflected from (or transmitted through) a sample being studied [11]. This change is dependent on the optical constants and the distance travelled through the medium. The principle of operation of the Woollam VASE used here, is shown by Figure 4–1.

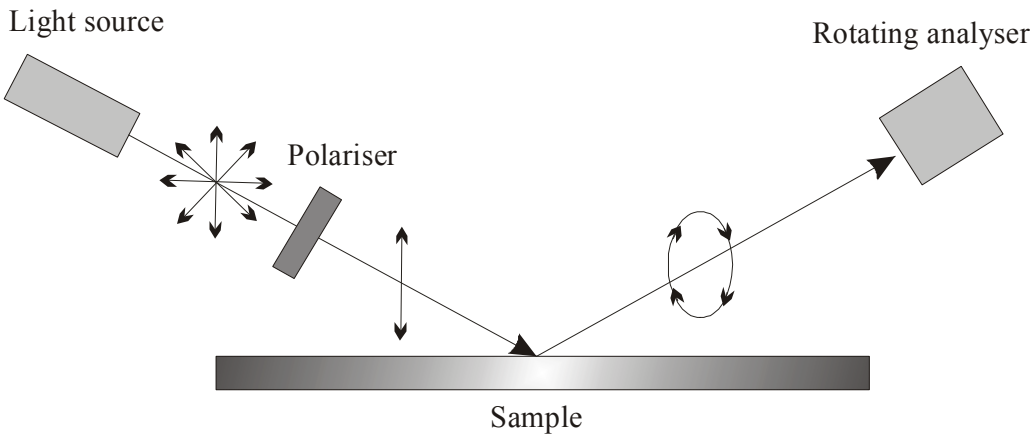

Figure 4–1. Operating principles of the Woollam ellipsometer

A light beam with a known initial polarisation (usually linear) is reflected from a sample that causes the light to become elliptically polarised. Two ellipsometric angles known as Ψ and Δ may be defined [12]. The angle Δ relates to the change in phase of the beam caused by the reflection; the angle Ψ relates to the change in amplitude caused by reflection. The electric vector is resolved into two components: parallel (p) to and perpendicular (s) to the plane of incidence, which is defined as the plane containing the incident and reflected beams and the vector normal to the sample surface. The ellipsometric angles are related to the Fresnel reflection coefficients [11] R_p and R_s through the equation of ellipticity, ρ:

Equation 4–1

$$\rho = \frac{R_p}{R_s} = \tan(\Psi)e^{i\Delta}$$

R_p and R_s can be related to the optical constants and the distance travelled through a medium. Appendix 1 gives a derivation of some of the equations used and describes the theory in greater detail. Under good experimental conditions, ellipsometry has been proven to be sensitive to sub-monolayer coverage on a surface [10].

4.2.3 Modelling process

In common with all optically based techniques, ellipsometry cannot be used to directly determine film thickness or a sample's optical constants. Instead, parameters are measured (Ψ and Δ) which are a function of the parameter of interest, as well as other parameters such as wavelength and angle of incidence which are measured. It then becomes necessary to build a model using the measured data, that incorporates the parameters of interest and that best fits the experimentally obtained results. Fitting is achieved through the minimisation of the difference between experimental and simulated data via a fitting algorithm.

A vital stage of this modelling process is to test that the best-fit parameters are unique, physically reasonable and are not strongly correlated. The confidence in this approach can be increased by the use of complementary data (determined by separate analytical techniques) that can be used in this modelling process to reduce the number of fitting parameters.

4.2.4 Variable angle spectroscopic ellipsometry

The ellipsometer used in this work is known as a Variable Angle Spectroscopic Ellipsometer (VASE). Experimental data can be acquired over a wide spectral range (between 190 nm and 1200 nm) at different angles of incidence [13]. This has two important advantages over earlier instruments that operated at a single wavelength and angle:

1. A large amount of data is collected which helps improve the confidence in the fitting process;

2. The spectral range and angles of incidence can be optimised for the determination of certain sample parameters, such as layer thickness or the optical constants of one of the films.

Typically, for samples studied in this work, a spectral range of 300 nm to 700 nm, with angles-of-incidences between 70° to 80°, have been used. These values have been selected to optimise the conditions for an oxide layer [11] by finding the condition where there is highest sensitivity, specifically near the Brewster angle.

4.2.5 Measurement of film thickness

The modelling strategy has been to adopt a simple structure of an oxide film on a silicon single crystal substrate. The presence of an amorphous structure, between the oxide and substrate, has also been modelled. Where this has led to an improvement in the quality of the fit, and is not strongly correlated with any of the fit parameters, it has been included. The assumed values for the optical constants of these two layers have been taken from the Handbook of Optical Constants of Solids [14]. For the oxide layer, values reported for bulk silicon dioxide (glass) have been used. Thus, a stoichiometry of SiO_2 is assumed. The amorphous (a-Si) optical constants are those reported for thin films (~600Å) that have been evaporated onto silicon single crystal substrates. The presence of an absorbed layer (§5.6) has not been modelled at this stage as its optical constants are unknown.

4.2.6 Focusing probes

The eventual aim of this work is the characterisation of surface films on 1 kg Avogadro spheres. These artefacts have a nominal diameter of 93 mm. The standard optics on the VASE system utilises a beam with an approximate diameter of 2.5 mm. This is ideally suited to flat surfaces and when an average of the measured parameters over a relatively large area is permissible (the footprint of the beam on a sample's surface at an angle-of-incidence of 75° is around 25 mm^2). However, to minimise potential errors due to oxide non-uniformity affecting the comparison of techniques, one needs to carefully control the measurement areas. Also, the divergence of the reflected beam from a spherical surface has led to a very poor signal-to-noise ratio at the detector, which may introduce large errors when estimating film thickness. Thus a means of reducing the beam spot was required and led to the installation, and thorough characterisation, of a pair of focusing probes. A description of this work has been included in Appendix 2.

4.3 Rutherford Backscattering Spectroscopy

4.3.1 Background

Rutherford Backscattering Spectroscopy (RBS) is a surface analysis technique that can be used to identify chemical elements and their concentration, as well as determining their depth from a surface. It is used in the near-surface region i.e. to a depth of a few micrometres. If the sample is a single crystal, then it can be used in a channelling mode (§4.3.5), which is sensitive to irregularities in the crystal lattice. In this work, RBS has been used to calculate the thickness of oxide layers (by assuming the oxide stoichiometry and atomic density) as well as damage to the lattice structure.

4.3.2 Principle

RBS is based on elastic collisions between projectile ions of a high energy (typically, several MeV) with atoms in the near surface region of a sample, at which the beam has been targeted [15]. It involves measuring the number and energy of ions (in this case alpha particles) that backscatter after the collision process. With this information it is possible to determine the atomic mass and elemental concentration against depth below the surface. Its sensitivity to low atomic number elements is relatively poor and is ideally suited for determining the concentration of trace elements that are heavier than the major constituents of the sample.

When a sample is bombarded with a beam of high-energy particles, the vast majority become implanted into the material and do not escape by scattering out of the target. This is because the diameter of an atomic nucleus is of the order of a femtometre (10^{-15} m) whilst the spacing between nuclei is around 2 Å (2×10^{-10} m). A small fraction of the incoming ions are backscattered from the nuclei of atoms in the upper few micrometres of the sample. This does not involve a direct collision. Rather an energy exchange occurs through the interaction of Coulombic forces between the nuclei, as they approach closely. This interaction can be modelled accurately as an elastic collision using classical physics. For scattering at a sample's surface, the only energy loss mechanism is momentum transfer to the target atom.

The ratio of the energy of the projectile after the collision $E_{scattered}$ to that of before $E_{incident}$ is called the *kinematic factor k*.

Equation 4–2

$$k = \frac{E_{scattered}}{E_{incident}} = \left[\frac{\left(M_2^2 - M_1^2 \sin^2 \psi\right)^{1/2} + M_1 \cos\psi}{M_1 + M_2} \right]$$

where M_1 is the mass of the incident ion, M_2 is the mass of the target atom and ψ is the backscattering angle measured from the incident path. Equation 4–2 can be used to calculate the mass of the target atom from measurements of the energy of backscattered ions, provided that the mass of the projectile ions M_1 and the incident energy are known. Thus, for a monoenergetic beam of ions of known energy, RBS is able to identify the target elements present at a surface through knowledge of their atomic mass.

4.3.3 Scattering cross-section $d\sigma/d\Omega$ and yield

The number of backscattering events that occur from a given element in a sample depends upon two factors, firstly, the concentration of the element and secondly, the effective size of its nucleus. The effective size of the nucleus is described by its scattering cross-section σ, and is proportional to the square of its atomic number. Figure 4–2 shows the backscattering process (in this example the reaction has taken place below the sample surface).

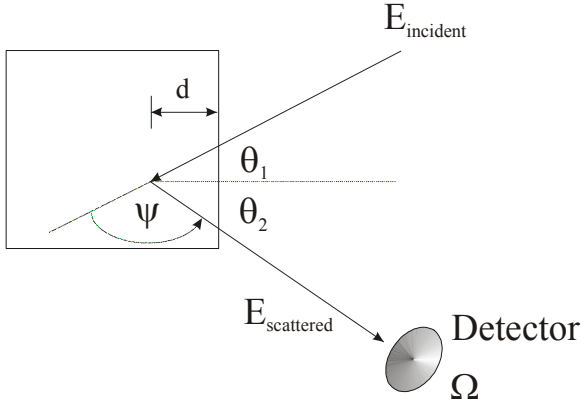

Figure 4–2. An ion backscattered from a nucleus at depth *d*

The backscattered ion has been observed at an angle ψ to the incident beam, using a detector that subtends a small solid angle Ω. The Yield Y (defined as the count rate at the detector) is given by:

Equation 4–3

$$Y = I\ N\ d\ \sigma_E\ \Omega\ \varepsilon$$

where I is the incident beam current (expressed as the number of ions per second), N is the atomic density of the sample, d is the target depth, σ_E is the scattering cross-section for a given incident energy E, and ε is the detector efficiency. Thus the total yield from the scattering experiment is directly related to the concentration of target atoms (RBS is sensitive to the product of N and d, referred to as the areal density).

4.3.4 Depth profiling

The situation for a particle that has travelled into the material becomes more complicated. Particles lose energy as they pass through a sample, both before and after collision, and can do so by a variety of physical mechanisms [15]. However, for incident energies of a few MeV one process is dominant. The energy loss arises from the interaction between the ion and the electrons of the atoms of the material, in the form of excitation and ionisation. This is termed *electronic stopping*. A particle that backscatters from an element at some depth in the sample will therefore have less energy than a particle that backscatters from the same element on the surface. The amount of energy a projectile loses per distance traversed (dE/dx) in a sample depends on the projectile's mass, its velocity, the elements in the sample, and the density of the sample material. A prior knowledge of dependence of energy loss on the sample composition and density enables measurements of layer thickness (or depth profiling).

4.3.5 Channelling

In addition to compositional information, RBS can be used to study the structure of single crystal samples. Channelling will occur when the rows or planes of atoms in the lattice are aligned parallel to the incident beam. The ordered electric fields produced by these planes act to guide or 'channel' the ions between the planes, preventing them from approaching individual nuclei and greatly reducing electronic stopping and the probability of backscattering (typically just a few percent of the signal obtained from a non-aligned or amorphous material). By measuring the reduction in the backscattering when a sample is channelled, it is possible to quantify the crystal perfection and to determine a single crystal's orientation in relation to the beam. Figure 4–3 demonstrates the reduction in yield when a crystal is channelled compared with the (upper) signal from an amorphous sample. The yield has been plotted against the detector channel number (an increasing channel number corresponds to an increasing energy of the backscattered ion).

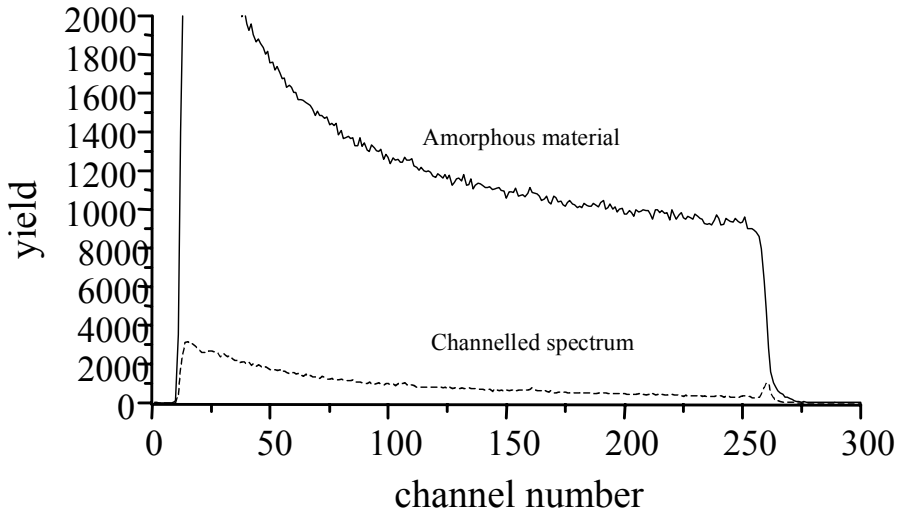

Figure 4–3. The yield from an amorphous sample compared with a channelled single crystal

Figure 4–4 shows a typical channelling spectrum obtained for a polished silicon sample with a native oxide. The general background signal corresponds to backscattered ions from silicon atoms within the crystal; their energy decreases with depth as energy is lost to inelastic scattering events (electron stopping). The yield increases with depth due to two mechanisms:

1) scattering cross-section is inversely proportional to the square of the ion beam energy; 2) ion beam becomes progressively de-channelled the further it travels into the crystal.

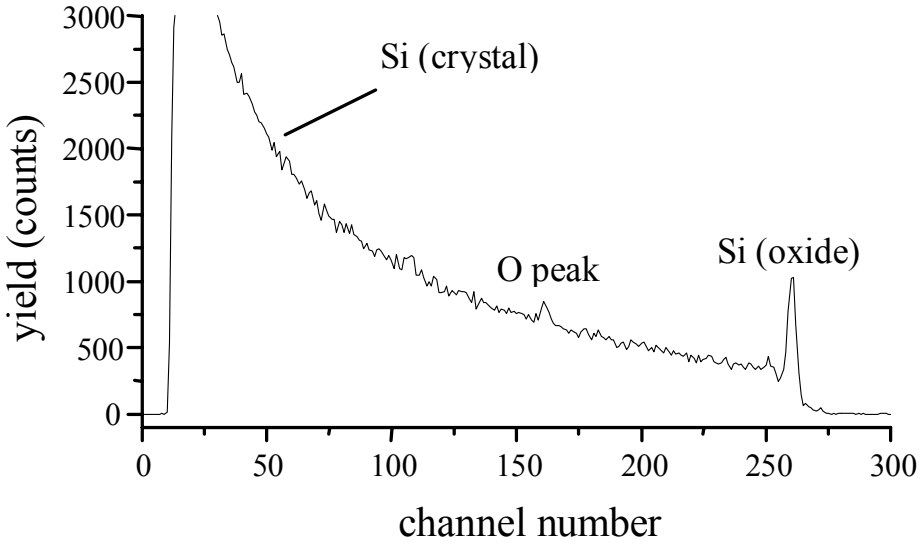

Figure 4–4. A channelling spectrum for an oxide on a silicon substrate

Two peaks are observed near channel numbers 260 and 160. The first of these corresponds to silicon atoms which are near the surface and within the oxide layer. The second peak is due to oxygen atoms within the oxide layer. This peak occurs at a lower energy as the mass of an oxygen atom is less than that of silicon, and more momentum is transferred to the oxygen atom when backscattering occurs. The yield of the silicon oxide peak is greater than the crystal because the oxide is amorphous and channelling only occurs within the crystal.

4.3.6 Measurement of oxide film thickness

For ultra thin films, the errors associated with calculating film thickness through energy loss calculations §4.3.4 become large due to the energy resolution of the detector. For this reason, the thickness of the oxide layer is calculated by another method. For a given spectrum, the total yield of oxygen atoms (i.e. area under the oxygen peak) is calculated. This is achieved by firstly subtracting the silicon background yield and then integrating under the oxygen peak. Equation 4–3 is then used to determine the areal density of oxygen atoms (i.e. the product of N x d, giving the number of oxygen atoms cm^{-2}). A stoichiometry of SiO_2 has then been assumed to estimate the total number of atoms cm^{-2}. This value is then converted to a

thickness measurement by assuming an atomic density of silicon dioxide of 6.6 x 10^{22} atoms cm^{-3}.

The RBS measurements were made using the instruments at the EPSRC ion beam facility at the University of Surrey and in Jena, Germany. The measurements at Surrey were performed using 1.5 MeV He ions. Measurements of the backscattering yield at Jena were further enhanced by using 3.05 MeV He ions. Resonance of the oxygen atom leads to an increased scattering cross section at 3.05 MeV.

4.3.7 Measurement of amorphous film thickness

The addition of an amorphous layer near a crystal's surface will cause a de-channelling of the ion beam, which leads to an increased backscattered yield. The effect of de-channelling is shown by Figure 4–5. The lower spectrum is that obtained for a damage-free crystal. The thickness of the amorphous layer can be quantified by comparing the two spectra.

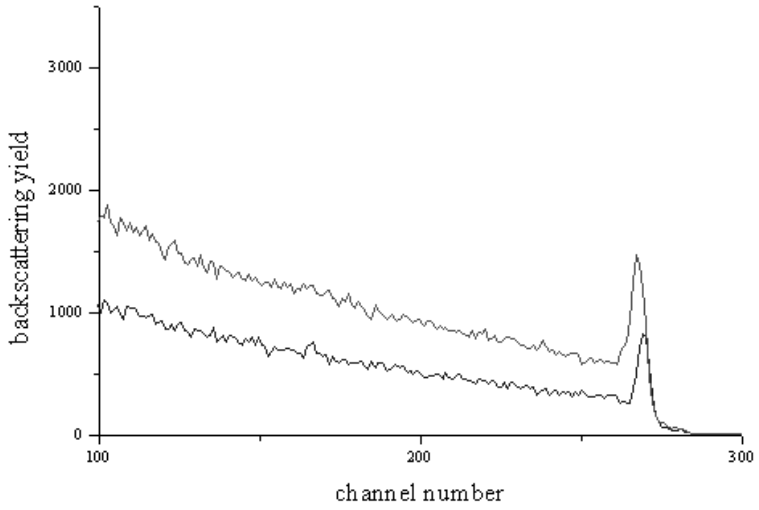

Figure 4–5. Increased backscattering yield due to presence of an amorphous layer. Undamaged crystal (bottom spectrum); crystal containing amorphous damage (top spectrum)

4.4 X-ray Photoelectron Spectroscopy

4.4.1 Background

X-ray Photoelectron Spectroscopy (XPS) is a technique that can be used to identify chemical elements on a surface and their electronic state, their relative numbers and depth. This analysis can be used to determine the thickness of thin films (typically less than 15 nm or so) on a substrate. Knowledge of an element's electronic state provides information on its chemical state. XPS is used to determine the thickness of the oxide layer and its stoichiometry (SiO_x) as well as information on the presence of any contaminants.

4.4.2 Principle of XPS

XPS derives its information through the energy analysis of low energy electrons (generally with kinetic energies in the range 20 to 2000 eV) emitted from the sample under investigation [16]. Electrons are emitted from the sample as a result of a photoemission process i.e. the ejection of an electron from a core level by an x-ray photon. The energy of the emitted photoelectrons is then analysed and the data presented as a graph of intensity (total number of counts) against electron energy. The basic components of an XPS system consist of a source of monochromatic x-rays (usually Al K_α) and an electron analyser. These are mounted within a vacuum system operating in the ultra-high vacuum range (below 10^{-6} Pa). Vacuum is necessary to de-sorb any loosely bonded contaminants (such as water molecules) from a specimen's surface that might otherwise prevent these photoelectrons from escaping and being detected. It also prevents further scattering of an electron by ambient gases. Figure 4–6 shows the process of photoemission. In this example, an electron from the *K shell* has been ejected from the atom. This electron is termed a *1s* electron.

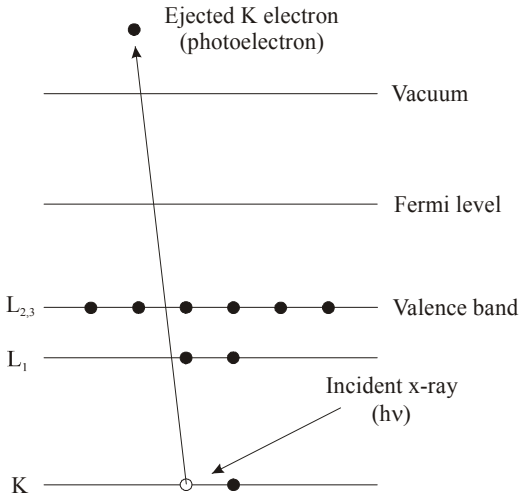

Figure 4–6. Photoemission of an electron by an X-ray

The kinetic energy E_K of the electron is the experimentally measured quantity. However, E_K is not an intrinsic property of the material. E_K is dependent on the energy of the x-ray as well as its electronic state in its parent element. Instead, the binding energy E_B is used to specifically identify the electron, both in terms of its parent element and atomic energy level. The binding energy is taken as a direct measure of the energy required to just remove an electron from its initial level to that of vacuum. The relationship between the energies involved in an XPS experiment can be written:

Equation 4–4

$$E_B = h\nu - E_K$$

where h is Planck's constant, ν is the photon frequency and their product $h\nu$ is the photon energy.

Figure 5–1 shows an example of a typical spectra generated by samples used in this investigation. The electrons that are excited and escape without energy loss contribute to the characteristic peaks in the spectrum; those that undergo inelastic scattering [16] and suffer energy loss, contribute to the background spectrum. As a result of this inelastic scattering process, not all electrons can escape and the probability of detecting an electron originating from a specific depth falls off exponentially with depth (Appendix 3). To characterise the

depth dependence of inelastic scattering, a parameter called the electron attenuation length λ_f is introduced. λ_f is a function of the energy of the photoelectron.

4.4.3 Calculation of film thickness

In order to calculate the film thickness, the attenuation length λ_f for the material must be known. In this work, the value for silicon has been taken from the work of Mitchell [17]. The presence of a carbonaceous layer on the silicon surface has also been identified (§5.6). To estimate the thickness of this layer an attenuation length for high density Poly(ethylene) (HDPE) has been assumed to describe the attenuation in the unknown layer [18]. The thickness d of a film has been calculated using the following equations.

Equation 4–5

$$d = \lambda_f \sin\theta \ln(1 + 1/Q)$$

where Q is given by

Equation 4–6

$$Q = (I_{s,d} / I_{f,d})\,(I_{f,\infty} / I_{s,0})$$

and θ is the take-off angle of the instrument (the angle of the x-ray beam measured with respect to the plane containing the sample's surface); $I_{f,d}$ is the measured intensity from a film of thickness d; $I_{f,\infty}$ is the intensity from an infinitely thick film; $I_{s,d}$ is the intensity of the substrate peak which is covered with a film of thickness d; and $I_{s,0}$ is the intensity from a film-free substrate. A film-free surface was prepared in-situ by removing the surface oxide with an ion milling process, which utilises a beam of argon ions to remove material by a sputtering process. Appendix 3 provides further details of the methodology.

4.4.4 Oxide stoichiometry

The oxide stoichiometry has also been determined using XPS. This is calculated by comparing the ratio of the measured intensities corresponding to silicon with an oxidation state of +4 (i.e. originating from the oxide) with that of the oxygen peak. These values are reported in Table 5-3.

4.5 Atomic Force Microscopy

4.5.1 Background

Atomic Force Microscopy (AFM) is an established technique [19] that can provide quantitative topographical information on a surface with very high resolution. Typically, less than 3 nm lateral and 1 nm [20] vertical resolutions can be achieved. An advantage of this technique is that it can be used under ambient conditions with little sample preparation being required. By comparison, electron microscopy is carried in out in a vacuum environment and an insulating surface must be coated with a metal to achieve conductivity. Moreover, electron microscopy cannot easily quantitatively measure surface roughness or other features. In this work, AFM has been used to provide quantitative feedback when developing the polishing techniques described in §2. Measurement of the surface roughness, and any predominant topographical features, is being established for flat and cylindrical artefacts (§5.9).

4.5.2 Principles of operation (Nanoscope III)

The AFM used in this work is a Nanoscope III manufactured by Digital Instruments. Its main components are shown by Figure 4–7. AFM senses the interaction force between a probe tip and the surface being investigated. The tip is mounted on a flexible cantilever and is scanned over a sample's surface in the x and y directions. The height of the tip is usually maintained at a few nanometres above the surface. A laser beam is focused on the backside of the cantilever where it is reflected onto a quadrant photodiode detector. The detection system can determine the angle of deflection of the beam as a function of lateral position on the surface. In most designs, the probe is mounted stationary whilst the sample is moved beneath it using a piezoelectric actuator.

A three-dimensional representation of the surface is achieved by monitoring the interaction between the tip and the sample as it scans over the surface. The interactive forces can be repulsive or attractive depending on the mode of operation and tip/sample interactions. For this work, two modes of operation have been used: contact and tapping.

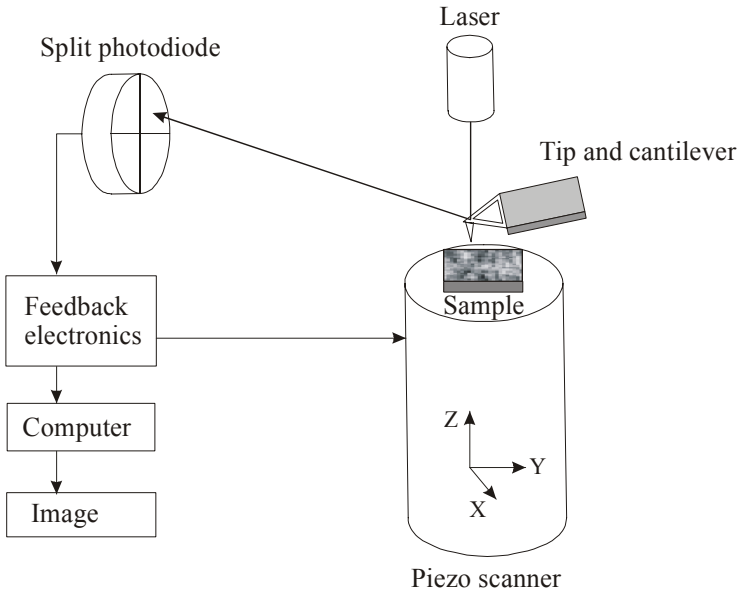

Figure 4–7. Schematic diagram of the components of the Nanoscope III

4.5.3 Contact mode AFM

The tip is in permanent contact with the sample in contact mode AFM. The term 'contact' is used here to describe the condition when the Coulombic forces between atoms of the tip and sample are encountered. Electron shells from atoms on the tip and sample repel one another, preventing further intrusion by one material into the other. If further force is exerted, then both tip and sample will be damaged. Thus, the forces being measured in contact mode are repulsive.

Topographical features on a sample's surface will deflect the cantilever, which in turn, will move the position of the beam spot across the photodiode. This change in position is used by the feedback circuitry to move the sample in the *z* direction to maintain a constant deflection of the cantilever, which is proportional to the height of the topographical feature.

4.5.4 Tapping mode™ AFM

In tapping mode AFM, the tip is made to oscillate near the cantilever resonance frequency (~100 kHz) using a piezoelectric crystal. When the tip is clear of the sample's surface its

amplitude of oscillation is unattenuated. As the tip is brought closer to the sample, the bottom-most point of each oscillation will come intermittently into contact with the sample i.e. it taps the sample. In this regime, the forces of interaction are attractive Van der Waals and the amplitude of the oscillation is now dampened. A feedback loop in this mode is used to maintain a constant amplitude of oscillation. Tapping mode is ideally suited for imaging soft biological samples where the higher forces of contact mode might damage the sample. This can equally apply to weakly bonded contaminants on a silicon surface that might be dislodged by contact mode. Furthermore, the variation of viscoelastic properties across a surface may be compared by phase imaging. In this mode, the phase lag between the signal that drives the cantilever oscillation and that detected by the photodiode is compared. Changes in phase lag reflect changes in the mechanical properties of the surface.

5 ANALYSIS OF RESULTS AND DISCUSSION

5.1 Previous studies on polished silicon surfaces

Present day knowledge of the structure and composition of a silicon surface that has been prepared using a mechanical polishing technique (§2.3) is very limited. The surface of silicon has been extensively studied due to its importance to the semi-conductor industry. However, the vast majority of this work is concerned with the characterisation of surfaces that have been chemically treated to produce a damage-free, atomically clean surface (often based on a modified RCA [21] technique to remove contaminants following manufacture and native oxides) followed by the growth of a stoichiometric thermal oxide [8],[22]. Furthermore, the crystallographic orientations are invariably that of (100) or (111).

Ellipsometry has been used to determine oxide thickness on polished silicon spheres by participating NMI's within the Avogadro project. However, the interpretation of the experimental data assumes the surface composition is made entirely of SiO_2 with no physical model for surface damage or adsorbed contaminants [3], [4] and [23]. Furthermore, the thickness has been calculated on the assumption that bulk optical constants of SiO_2 apply to the native oxide.

5.2 Surface geometry

An objective of this work is to establish ellipsometry as a stand-alone technique for the measurement of the thickness of contaminating layers on polished silicon spheres (§4.1). Accommodation of a silicon sphere is relatively straightforward and the measurements can be carried out in ambient conditions. The RBS and XPS instruments at the University of Surrey, in common with most facilities, are not equipped with a goniometer stage that can handle a 1 kg silicon sphere.

The first samples to be successfully polished at NPL were those with a flat surface (§2.3.1) and have been used as a basis for a comparison of the described analytical techniques. However, the surface of a sphere will be comprised of many exposed crystallographic planes

whereas the flats consist of only a single plane. To investigate the impact of polishing on different crystallographic planes, flat surfaces have been used with different crystallographic orientations. Silicon has a diamond face-centred-cubic structure [9]. The crystallographic planes (100) and (111) represent the two extremes of this structure when one considers the density of atoms per unit area, with the (111) plane being the most dense. Further orientations of (110), (211) and (311) have also been included in this study.

5.3 Measurement uncertainties and assumptions

The uncertainty in the measurement of the thickness of contaminating layers has yet to be evaluated for any of the analytical techniques. In the following analysis, comparisons between these techniques have been made. Although differences have been reported, it is not possible to comment on their agreement in terms of experimental uncertainty.

All the measurement techniques (VASE, RBS and XPS) make certain assumptions when determining the thickness of these ultra thin surface layers. These assumptions have been summarised in Table 5-1.

Measurement technique	Assumptions
VASE	Optical constants of bulk silicon dioxide and amorphous silicon (deposited by evaporation) have been taken as applying to the native oxide and amorphous layer respectively.
RBS	Calculations of native oxide thickness have been based on an assumed atomic density of a bulk thermal oxide, with a stoichiometry of SiO_2.
XPS	Calculations of native oxide thickness have been based on an assumed atomic density and attenuation length, determined for a bulk thermal oxide. Attenuation length for high density Poly(ethylene) has been used to determine thickness of carbonaceous layers

Table 5-1: Assumptions concerning the physical properties of ultra thin layers made using each measurement technique

5.4 Film thickness measurements

Table 5-2 gives a summary of the measurements of the thickness of contaminating layers on silicon substrates that have been made to date. They include a range of different samples, polished along different orientations, with several surface treatments. The main surface of interest is that of samples that have been polished at NPL and a native oxide left to form. Other treatments have been included for comparative purposes. The nomenclature used in Table 5-2 to indicate the different methods of treatment is:

- cmp = chemical mechanical polishing. A technique developed by the semiconductor industry to polish silicon wafers. It involves a combination of mechanical polishing (often under high pressure and temperature to reduce polishing time) and chemical etching.
- npl = polished at NPL using the method described at (§2.3)
- therm = a thermally grown oxide[5]
- native = oxide formed in ambient conditions
- sput = an in-situ XPS technique to sputter an oxide from a surface revealing the bare silicon substrate. This technique utilises a beam of argon ions with an energy of 3 keV.

The samples have a surface area of around 1 cm^2. Under the 'sample identification' column, the labelling a, b or c refers to measurements made at different locations on a given sample.

[5] Typically, a wafer is oxidised following some form of pre-treatment (i.e. RCA clean) in a dry oxygen environment at a temperature around 800°C. The duration of this treatment is used to control the thickness of the oxide layer.

Sample identification	Crystal orientation	Treatment	VA(SE)		XPS		RBS (Jena)		RBS (Surrey)		Difference in oxide thickness		
			Thickness (Å)		Thickness (Å)		Thickness (Å)		Thickness (Å)		se-xps	se-rbs	xps-rbs
			oxide	a-si*	oxide	carbon	oxide	a-si*	oxide	a-si*	(Å)	(Å)	(Å)
s(v1)a	100	cmp / therm	169.2	0.0	-	9.0	-	-	155.0	0.0	-	14.2	-
100(E)a	100	cmp / native	42.5	0.0	-	-	16.4	0.0	-	-	-	26.1	-
110(D)a	110	cmp / native	33.3	0.0	-	-	16.5	0.0	-	-	-	16.8	-
111(B)a	111	cmp / native	37.6	0.0	10.2	6.7**	19.1	0.0	-	-	27.4	18.5	-8.9
211(C)a	211	cmp / native	39.4	0.0	11.8	5.3**	18.0	0.0	-	-	27.6	21.4	-6.2
311(A)a	311	cmp / native	38.8	0.0	12.2	5.3**	15.6	0.0	-	-	26.6	23.2	-3.4
100(T2)a	100	npl / native	42.1	3.9	10.6	8.2	14.1	18.0	-	-	31.5	28.0	-3.5
110(T2)a	110	npl / native	32.8	2.2	-	-	11.2	0.0	-	-	-	21.6	-
111(T3)a	111	npl / native	39.3	4.0	-	-	12.0	22.0	-	-	-	27.3	-
211(T2)a	211	npl / native	29.9	8.1	13.0	10.0	11.1	42.0	-	-	16.9	18.8	1.9
211(T2)b	211	npl / native	35.4	7.4	13.0	9.8	-	-	-	-	22.4	-	-
211(T2)c	211	npl / native	34.0	7.1	12.5	9.3	-	-	-	-	21.5	-	-
311(T3)a	311	npl / native	34.5	5.2	8.4	7.5**	12.6	34.0	-	-	26.1	21.9	-4.2
10(v2)a	100	cmp / native	31.2	0.0	11.0	9.4	-	-	16.5	0.0	20.2	14.7	-5.5
10(v2)b	100	cmp / native	34.5	0.0	9.4	9.2	-	-	-	-	25.1	-	-
10(v3)a	100	sput / native	-	-	14.3	6.6**	-	-			-	-	-
10(t3)a	100	npl / native	-	-	-	-	-	-	10.0	0.0	-	-	-
10(t5)a	100	npl / native	45.3	0.0	12.8	12.6	13.5	0.0	11.0	0.0	32.5	31.8	-0.7
10(t5)b	100	npl / native	39.2	0.0	12.2	12.6	-	-	-	-	27.0	-	-
10(t5)c	100	npl / native	38.9	0.0	12.9	12.9	-	-	-	-	26.0	-	-
9(1)a	100	npl / native	34.3	0.0	8.5	10.4	-	-	-	-	25.8	-	-
9(1)b	100	npl / native	32.6	0.0	8.7	10.1	-	-	-	-	23.9	-	-
9(1)c	100	npl / native	34.2	0.0	8.1	10.7	-	-	-	-	26.1	-	-
2(t1)a	unknown	npl / native	36.7	0.0	10.2	11.6	-	-	-	-	26.5	-	-
2(t1)b	unknown	npl / native	38.1	0.0	11.3	10.1	-	-	-	-	26.8	-	-
									AVERAGE		25.5	21.9	4.3

* a-si refers to 'amorphous silicon layers'
** cleaned immediately prior to undergoing XPS analysis (§5.6)

Table 5-2. Measurements of the thickness of contaminating layers on silicon substrates

5.5 Oxide layer

5.5.1 Agreement between the analytical techniques

All three analytical techniques have been used to determine the thickness of oxide layers. The methods used to calculate the thickness, and any assumptions that have made, have been described in §4. The final three columns of Table 5-2 report the differences between these techniques on the same sample. The average value of the magnitude of these differences has also been determined. In general, RBS and XPS are in reasonable agreement in determining values in the range 8-15 Å for samples polished at NPL. The comparison with VASE has been much poorer, with ellipsometry predicting values in the range 29-46 Å for the same samples.

5.5.2 Comparison of RBS and XPS

The average difference between the RBS and XPS measurements is 4.3 Å, with the largest discrepancy being 8.9 Å. With one exception, the XPS values are all lower than those of RBS. Although the measurement uncertainties have yet to be evaluated (§5.3) both of these techniques should be capable of determining the absolute thickness with an accuracy of better than 20% [24]. The reason for these discrepancies may be partly attributed to certain assumptions made during the RBS calculations (§4.3.6). These are 1) all the oxygen is assumed to be in the silicon oxide layer, 2) the silicon oxide is stoichiometric (i.e. SiO_2) and 3) the density of the silicon oxide is the same as that of amorphous SiO_2 in the bulk and has been taken as 6.6×10^{22} atoms cm^{-3}. Certainly some oxygen will be found in the carbonaceous layer that has been identified (§5.6) and the stoichiometry may be greater than 2 due to the inclusion of hydroxyl bonds within the oxide [25]. Both of these assumptions may artificially increase the thickness of the value of the oxide layer predicted by RBS. The XPS calculations have assumed an attenuation length in silicon oxide that is based on amorphous SiO_2 in the bulk.

5.5.3 Previous study on native oxide thickness

A study of the growth of native oxides has been made by Raider [26] on etched silicon surfaces. Raider measured the oxide thickness using single wavelength ellipsometry and XPS. A discrepancy was found between these techniques. The values obtained by ellipsometry were around 10Å greater than that of XPS. This discrepancy was partly explained by the loss of physisorbed contaminants when the samples were placed in vacuum. The growth rate of the oxide layer followed a logarithmic relationship with time and no significant increase were observed after two weeks had elapsed. It was concluded that the thickness of the native oxide layer that grows on an etched silicon surface exposed to ambient conditions is less than 14Å. This result is consistent with the measurements made in this study by RBS and XPS.

5.5.4 Ellipsometry values

It would appear from the results described above that the ellipsometry values are too high. Part of this discrepancy is easily explained by the fact that XPS has been able to distinguish between an oxide and a carbonaceous layer, the latter with a thickness of around 10 Å (§5.6). For the VASE measurements, these two layers have been effectively modelled as a single oxide layer. This situation arises particularly when the optical constants of the carbonaceous layer are similar to those of the oxide and there is no optical contrast to cause a reflection from the interface. A discrepancy of around 15 Å still remains. The RBS measurements rely on the process of converting the counted areal density of the oxygen atoms into an oxide thickness and are, therefore, not effected by the presence of non-oxide contaminants. An error in the density value would lead to an equivalent error in the thickness.

There will also be a contribution to the discrepancy due to weakly bonded contaminants, such as water and hydrocarbons, that are desorbed from the surface when entering the RBS or XPS vacuum systems. The Council for Scientific and Industrial Research (CSIRO) in Australia has made measurements on the water uptake [3] of silicon spheres manufactured for the Avogadro project. Their conclusion was that under normal laboratory conditions (50% relative humidity), the uptake is about one monolayer (~3 Å). The contribution due to other loosely bonded contaminants is unknown at this stage.

Finally, another contribution to the discrepancy might lie in the assumed values of the optical constants used when modelling the VASE data. As stated previously, this data is based on values established for bulk samples of fused silica (§4.2.5). According to XPS analysis, the composition of the native oxide after polishing is non-stoichiometric (§5.8). If the refractive index of this non-stoichiometric oxide is lower than that of the bulk material used in the model, then the VASE analysis would over-estimate the thickness. All of these considerations clearly demonstrate the need to fully understand the sources of experimental uncertainty if absolute comparisons of oxide thickness are to made with an uncertainty of a few Ångstroms.

5.5.5 Variation with crystal orientation

Measurements made at CSIRO [3] on a polished silicon sphere have identified a variation in the oxide thickness that is correlated with crystallographic orientation. An ellipsometer was used to determine the oxide thickness at different locations on a sphere's surface. The mean values along the three principle crystallographic directions <100>, <110> and <111> were found to be 74, 85 and 94 Å respectively [3]. The cause of this variation is unknown.

In this study, measurements have been made on a set of silicon wafers that have been cut and polished along the crystallographic planes (100), (110), (111), (211) and (311) (§5.2). These were all prepared from a single boule and were treated in same manner i.e. CMP polished followed by growth of a native oxide. The miscut of the surfaces is unknown. For thoroughness, measurements were made on these wafers in the as-received condition. The wafers were then polished at NPL, removing sufficient material during the smoothing stages to ensure that no surface damage from their original treatment remained. The results of the oxide thickness measurements are shown by Graph 5-1.

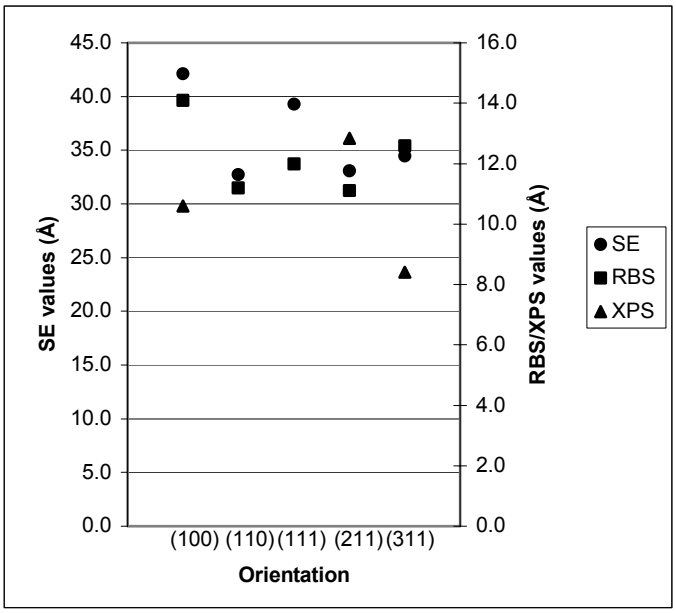

Graph 5-1. Variation of oxide thickness with respect to crystallographic orientation

VASE and RBS measurements have been made on each of the orientations. The XPS measurements have been limited to three orientations, namely (100), (211) and (311). The variation with crystallographic orientation, as determined by VASE and RBS, is broadly correlated and is illustrated by Graph 5-2 but systematically different by about 20 Å. The trend reported by CSIRO is not seen here. However, it is impossible to draw any conclusions at this stage: error bars corresponding to the uncertainty of each technique have yet to be determined; the reproducibility of the polishing process has not been established; and the uniformity of oxide thickness across a signal wafer is unknown. Concerning this latter point, two samples with (100) orientations, and one with a (211), have had XPS measurements made at three locations that are spaced approximately 0.5 cm apart. In each case, the variation in oxide thickness has been less 1 Å.

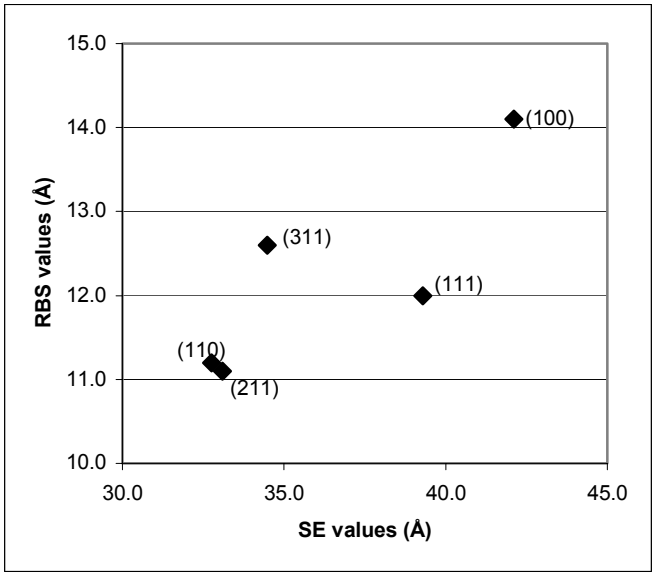

Graph 5-2. Correlation between the RBS and SE measurements

The polishing and measurement procedure will be repeated for a second set of wafers with different orientations (§6.3.2). This will provide further information on the agreement between these techniques and the reproducibility of the NPL polishing process that is applied to flat wafers. However, the main interest of the Avogadro project lies with the measurement of polished spheres. The chemical and physical processes involved in polishing a sphere are different from that of a flat: the polishing slurry and lap are different, as too is the applied pressure. Furthermore, a sphere will have many crystallographic planes exposed. The surface of two spheres will be characterised, both in terms of the thickness and variation of contaminating layers with respect to the crystallographic orientation, and the reproducibility of the polishing technique (§6.5).

5.6 Carbonaceous layer

The samples were cleaned using a common procedure prior to their analysis by any of the described techniques. For samples polished at NPL this was necessary to remove any visible residue remaining after the final polishing stage (§2.3). The samples were cleaned by soaking a cotton-tipped bud with ethanol and, with a firm pressure, wiping over their surface. They were then stored at room temperature, in containers manufactured from Styrene, for timescales varying between a few weeks to a few months before analysis by XPS. Samples marked with an ** in Table 5-2 were cleaned a second time, immediately prior to the XPS measurements.

Figure 5–1 shows the results of an XPS survey scan on a sample that has been polished at NPL. This result was representative of those obtained for all surfaces. Only three elements have been identified (in any significant amount) on the surface. They are silicon, oxygen and carbon.

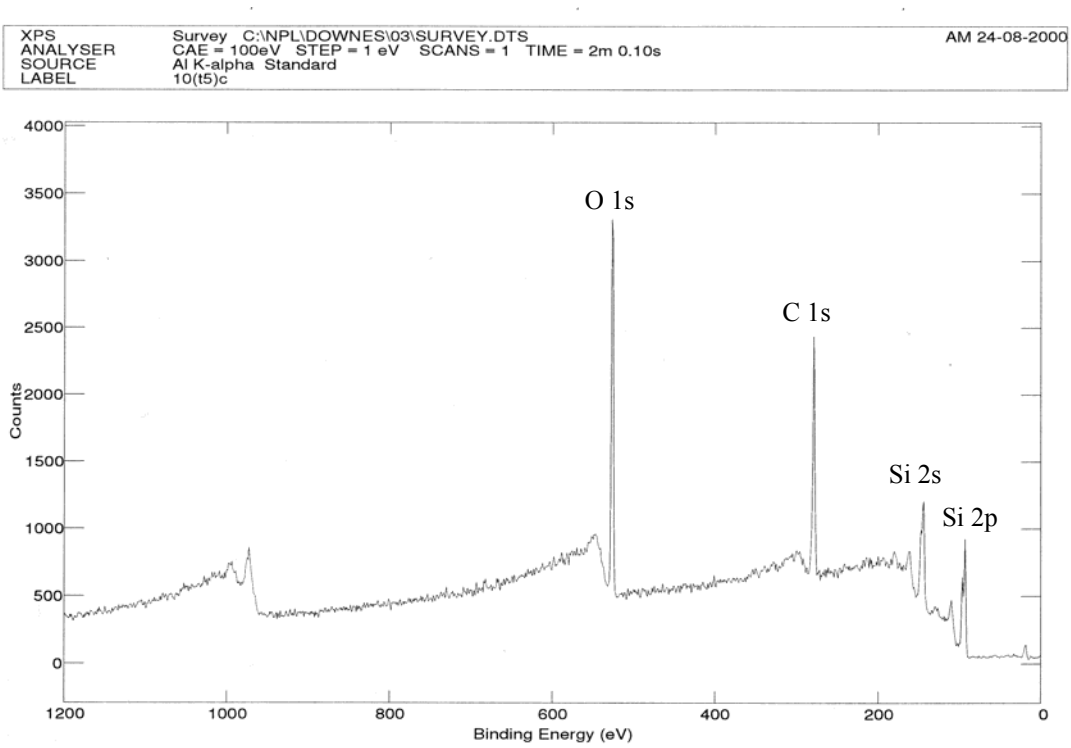

Figure 5–1. Survey scan of contaminants on a NPL polished silicon substrate of (100) orientation

The carbon peak corresponds to the presence of carbonaceous contaminants which are to be expected for any surface that has been exposed to ambient conditions. Carbonaceous contaminants fall into four distinct functional groups [27] given by hydrocarbon (C-H), alcohol (C-OH), ketone (C=O) and carboxylic acid (COOH). Figure 5–2 shows the carbon peak in greater detail, together with the fitting process that has identified the four peaks (labelled A, B, C and D respectively) that correspond to these groupings. As would be expected, hydrocarbon contaminants are the most abundant.

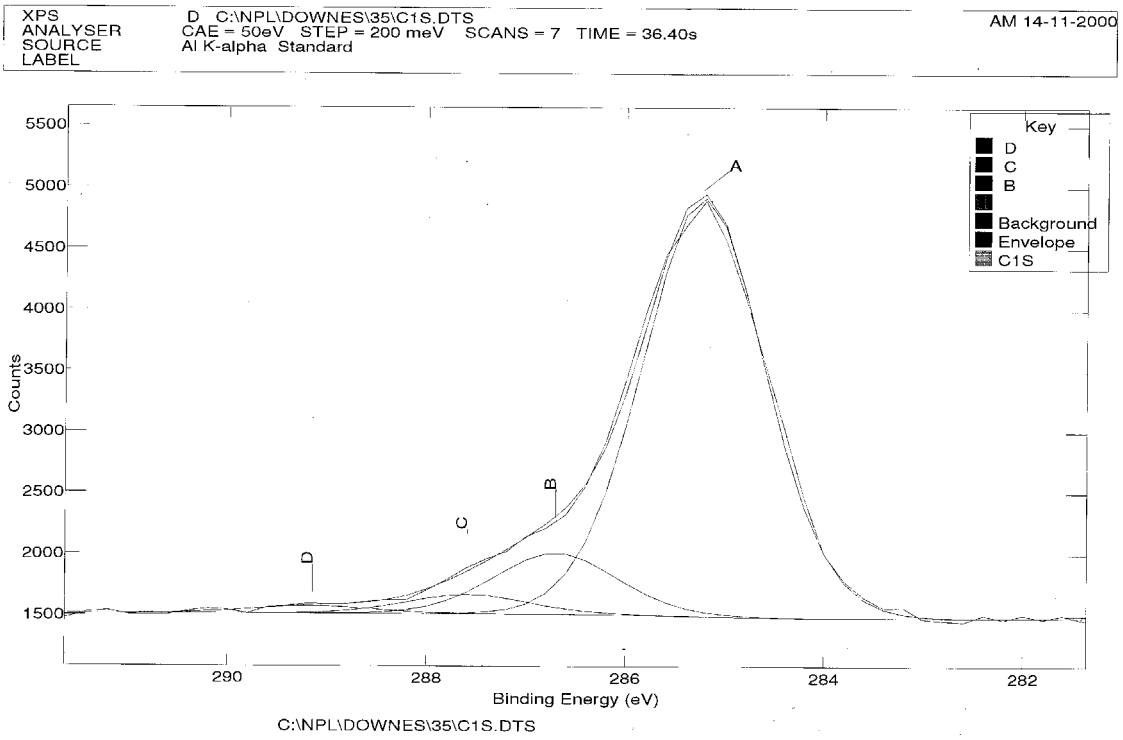

Figure 5–2. Peak fit of the carbon C 1s signal

Due to the nature of oxide growth [8] (i.e. progressively moving into a crystal) these contaminants will be found on the surface of the oxide. The thickness of these layers has been determined as described in (§4.4.3). Many of the samples have been analysed at several different locations on their surface. This has confirmed that the carbonaceous layer can be treated as being of uniform thickness; the maximum variation across any sample was 0.7 Å. The thickness of this layer was in the range 8 to 13 Å for all samples that had been cleaned at least 4 weeks prior to measurement. For the freshly cleaned samples the range was 5 to 8 Å. This would indicate that the cleaning process was effective at removing 3 to 5 Å of relatively

strongly bonded contaminants (weakly bonded hydrocarbons and water are expected to be removed by the vacuum).

The next stage will be to identify the composition of the function groups that make up a surface polished and prepared in this manner (§6.2). Storage of these surfaces will be in glass containers to avoid possible contamination of the surface by the Styrene containers. A substance (most likely a polymer due to the strong hydrocarbon presence) that best matches the composition will be identified and its optical constants substituted in the ellipsometer modelling process. In this manner, ellipsometry may have the necessary sensitivity to separate the contributions from the silicon oxide and carbonaceous layers.

5.7 Damage to the lattice structure

RBS channelling measurements have been made on six wafers that have been re-polished at NPL. Damage to the crystal lattice has been detected on four of these wafers with orientations of (100), (111), (211) and (311). Furthermore, the data indicate that the silicon has an amorphous form near its surface. The damage can be attributed to the mechanical polishing process used at NPL. Measurements were made on these wafers in the as-received condition (i.e. surface prepared using a Chemo Mechanical Polishing process) and no damage was detected. For the same four samples, the VASE fit was also significantly improved by the inclusion of an amorphous layer between the oxide and the substrate. It was also possible to model an amorphous layer on the remaining (110) sample though the improvement in the fit was relatively small.

The thickness of these amorphous layers is shown by Graph 5-3. With the exception of the wafer with a (110) orientation, with its low level of damage, the thickness calculated by RBS was greater than that determined by ellipsometry. However, there was a strong degree of correlation between these two techniques that can be seen in Graph 5-4. As seen previously with the oxide layer, wrongly assumed values of the optical constants used in the ellipsometry model may explain part, or all, of this discrepancy.

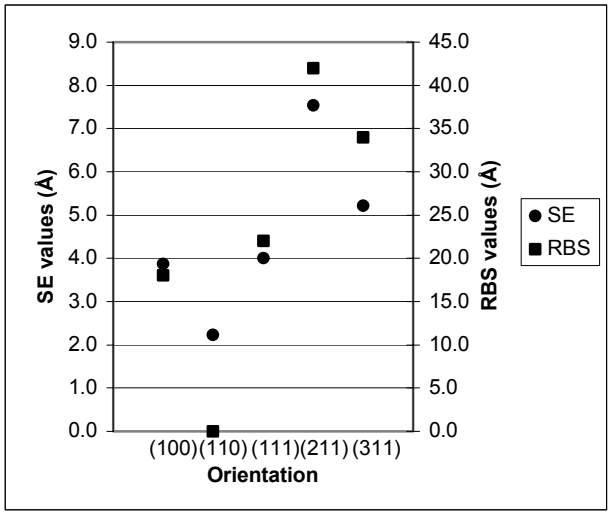

Graph 5-3. Variation of amorphous damage with crystallographic orientation

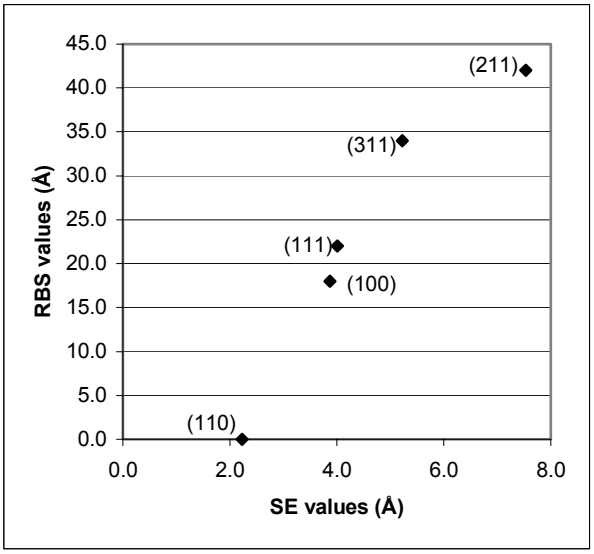

Graph 5-4. Correlation between RBS and SE measurements of amorphous damage

The ellipsometry data will be re-modelled to determine if a consistent set of optical constants can be identified for an amorphous structure arising from the mechanical polishing process (§6.4). The thickness of the amorphous layers determined by RBS will be used in the VASE modelling. It is expected that the refractive index of the damaged region is different than that of amorphous silicon deposited by evaporation.

5.8 Oxide stoichiometry

Table 5-3 reports the measurements of oxide stoichiometry made using XPS (§4.4.4). The stoichiometry of each sample has been determined by calculating the ratio of the peak areas corresponding to silicon, with an oxidation state of +4, and oxygen (§4.4.4). It has been assumed that all the oxygen is found within the oxide. The data have been corrected for the sensitivities of silicon and oxygen. The sensitivity of an element is related to the probability of a photoemission event occurring.

Sample	Orientation	Stoichiometry (ratio O/Si)	Surface preparation (§5.4)
S(v1)	100	2.3	cmp / therm
10(v3)	100	2.6	sput / native
10(v2)	100	3.2	cmp / native
111(B)	111	3.8	cmp / native
211(C)	211	3.6	cmp / native
311(A)	311	3.5	cmp / native
10(t5)	100	2.9	npl / native
9(1)	100	3.9	npl / native
100(t2)	100	3.5	npl / native
211(t2)	211	2.6	npl / native
311(t3)	311	3.6	npl / native

Table 5-3. Measurement of oxide stoichiometry

All the samples measured have a stoichiometry greater than 2 (i.e. they are non-stoichiometric). Sample s(v1) is a wafer that has undergone a CMP process followed by the growth of a thermal oxide with a thickness of around 16 nm. One would expect the stoichiometry of this oxide to be 2. The measured value is 2.3, which may be an indication that one or both of the sensitivities for silicon or oxygen are incorrect. However, even allowing for a systematic error of +0.3, the measured stoichiometries for the surfaces with native oxides are higher than expected.

A silicon oxide containing silanol groups (SiOH) will have a stoichiometry greater than 2 according to the relationship $SiO_X(OH)_Y$, where 2X+Y=4. Hence a value of 3.9 nearly corresponds to silicic acid $Si(OH)_4$ and is unrealistic.

5.9 Surface topography

5.9.1 Standards

At the start of each day's measurements (or when a new tip is used) the performance of the AFM is checked against a reference silicon grating[6]. This standard has been supplied with a traceable step height of 25 nm and an associated uncertainty of ±1.0 nm (at a coverage factor k=1). The period of the gratings has been stated on the calibration certificate as 3.0 μm but no uncertainty in this dimension is given. Figure 5–3 shows a typical image obtained of the standard together with a sectional analysis (Figure 5–4) showing the measured step height and period. If necessary, the sensitivity of the piezo scanner is adjusted in the vertical and horizontal planes until the measured period of the grating is within ±1.0 nm and ±100 nm respectively of the stated values.

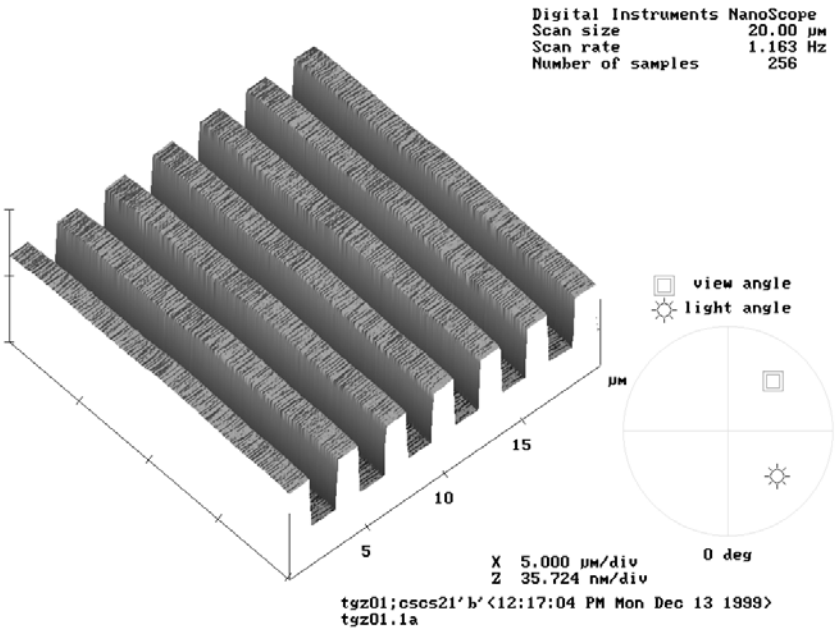

Figure 5–3. A 3-D topographical image of a reference grating. The scan size 20 μm.

[6] Provided by NT-MDT Molecular Devices and Tools for NanoTechnology. Traceability of the step-height is through the National Institute of Standards and Technology (NIST), USA.

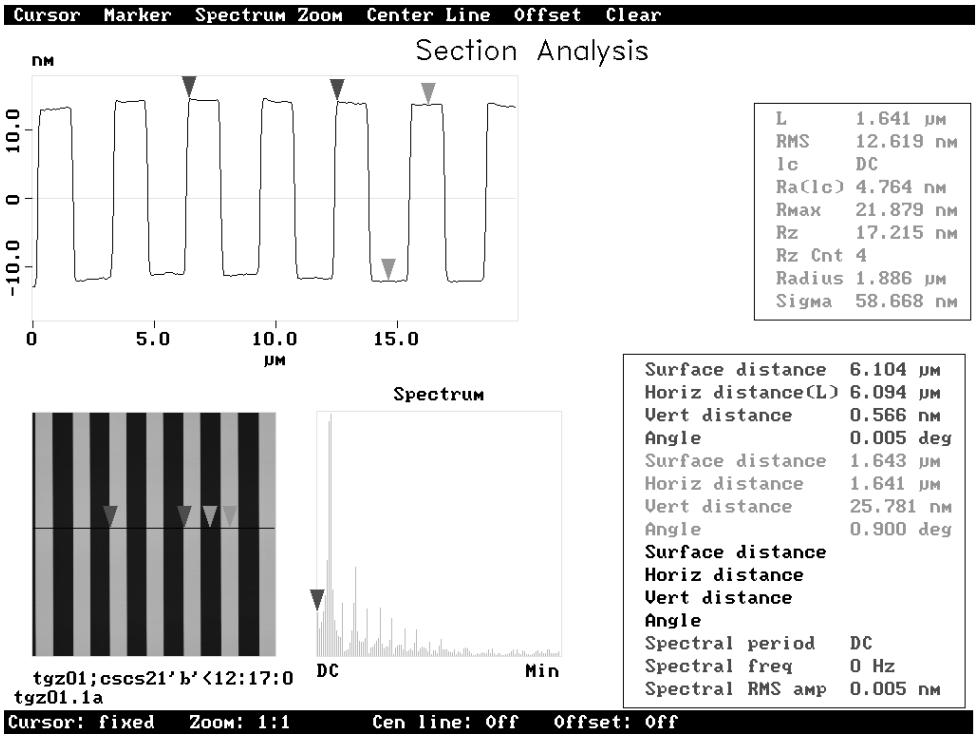

Figure 5–4. Sectional analysis of scanned area of reference grating. The depth of the grating has been measured as 25.8 nm, with a period of 3.0 µm

5.9.2 Flat surfaces

5.9.2.1 Surface features

Figure 5–5 shows two images, at different scales, of a surface that has been polished at NPL. This surface was cleaned with cotton wool soaked with ethanol following its removal from the polishing lap.

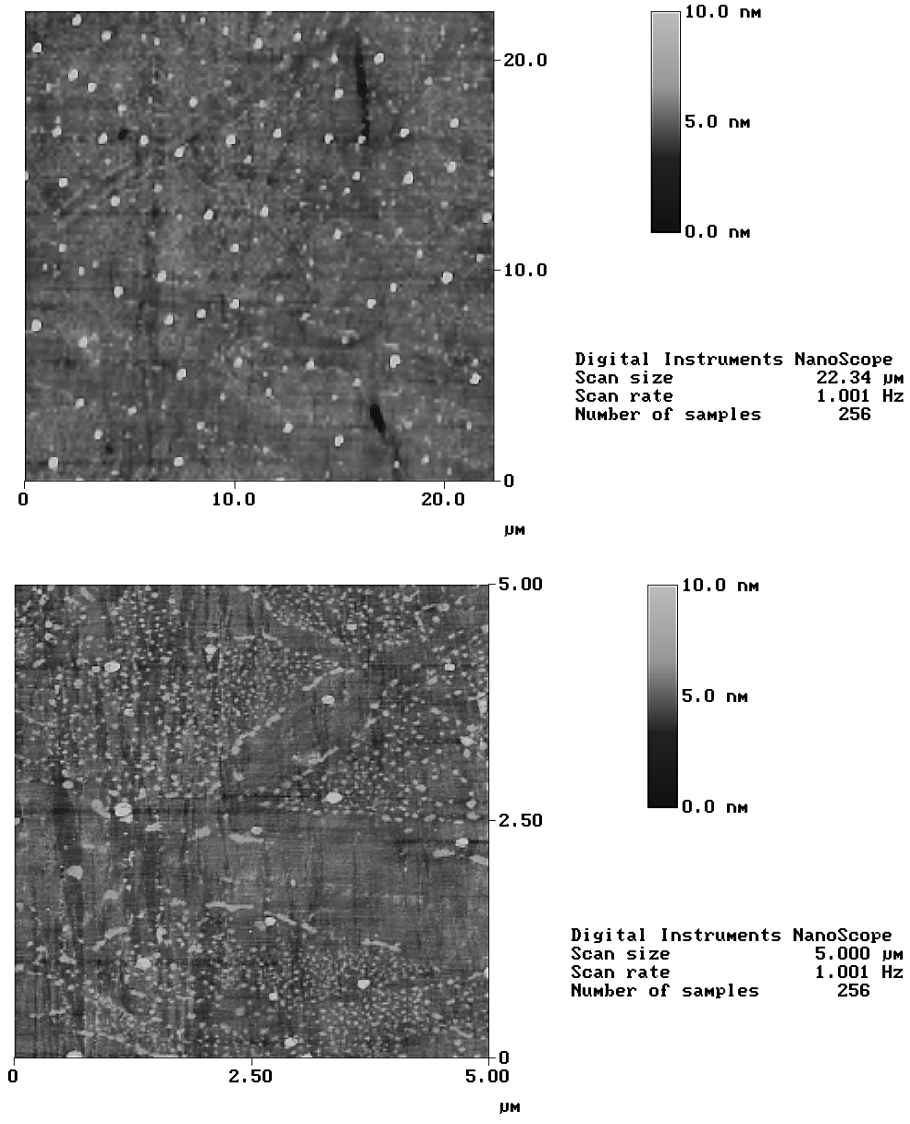

Figure 5–5. Topographical images of a polished silicon surface at two different scales: scan size of 22.3 µm (top) and 5 µm (bottom).

Several features can be seen at these magnifications and can be broadly categorised as either i) particulates ii) scratches/sleeks or iii) pitting to the surface. The scale and occurrence of the scratching and pitting is very low and is negligible when considering contributions to the surface roughness. The particulate contaminants, however, are more significant and increase the overall surface roughness as well as providing possible sites for the adsorption of further contaminants. Measurement of the Roughness average *Ra* yields values in the range 0.5 nm to 1 nm; when excluding these particulates *Ra* is 0.2 nm to 0.3 nm, a relative reduction of two or threefold.

The particulates have two distinct sizes. A sectional analysis (Figure 5–6 and Figure 5–7) shows the larger structures have heights of the order 5 to 10 nm and widths of 100 to 150 nm. The smaller structures have heights of the order 1 to 2 nm and widths of 20 to 50 nm.

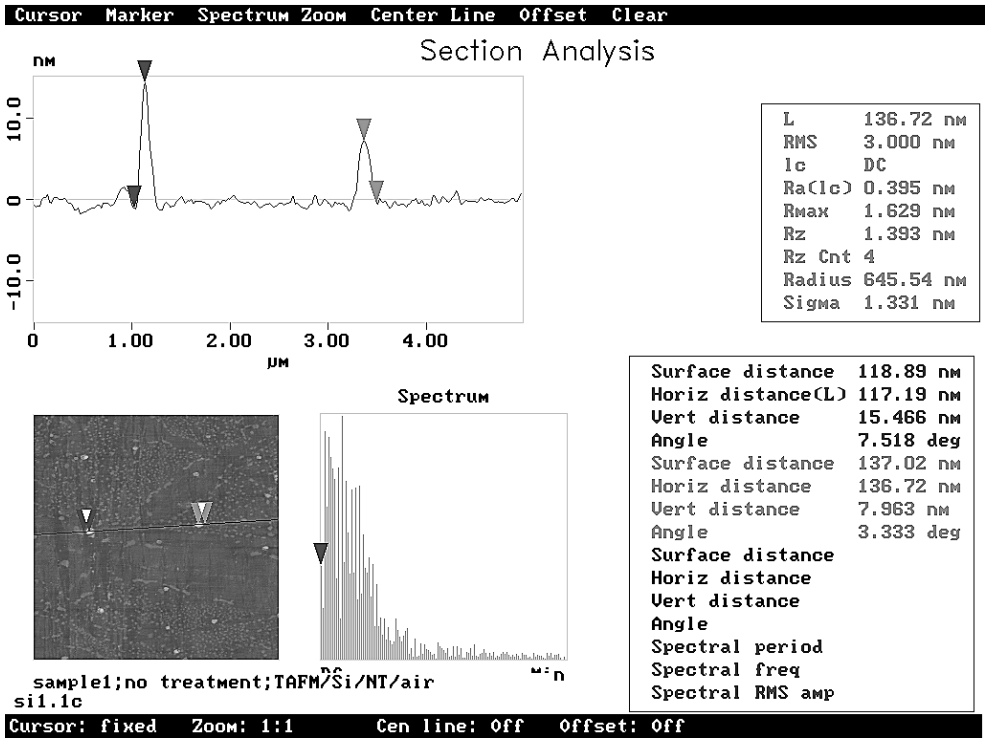

Figure 5–6. Sectional analysis of 'larger' particulate structures

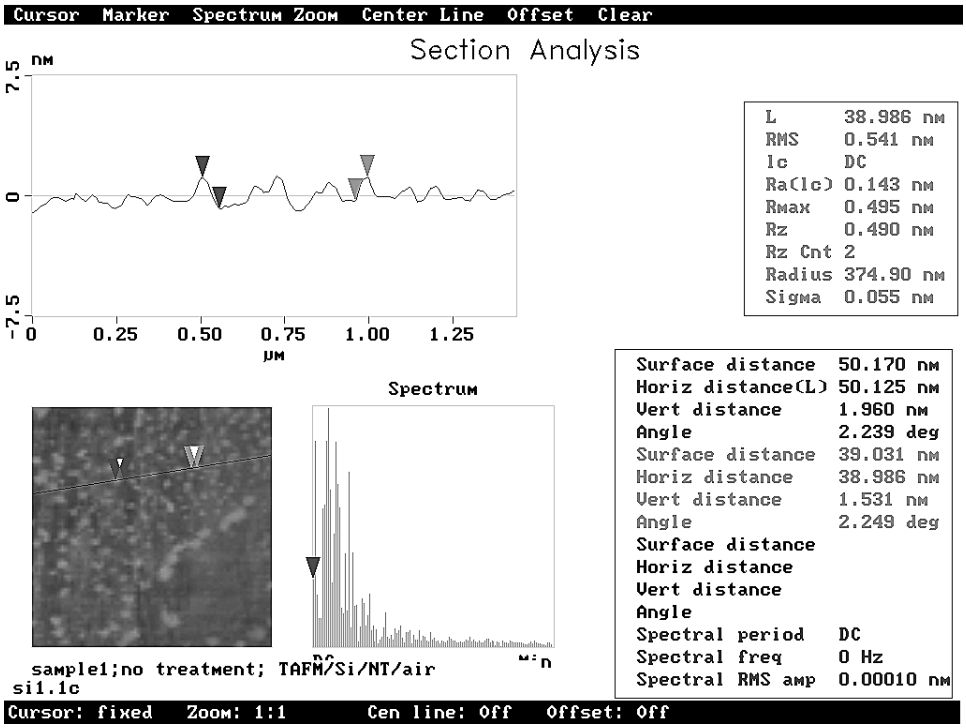

Figure 5–7. Sectional analysis of 'smaller' particulate structures

Figure 5–8 shows an area that has been scanned using the phase imaging mode of the instrument (§4.5.4). There is a clear phase difference between the large particles and the background oxide, suggesting that the contaminants have different viscoelastic properties than the oxide. For the smaller contaminants, this contrast is negligible suggesting similar viscoelastic properties to the oxide. These structures do have the appearance of drying stains; perhaps areas of silicon that are terminated with hydroxyl bonds. A possibility for the larger particles is that they are remnants of the aluminium oxide particles used in the final polishing stage. However, the information gained from the phase imaging is purely qualitative. The precise relationship between the elasticity of a material and the resulting phase shift is unknown.

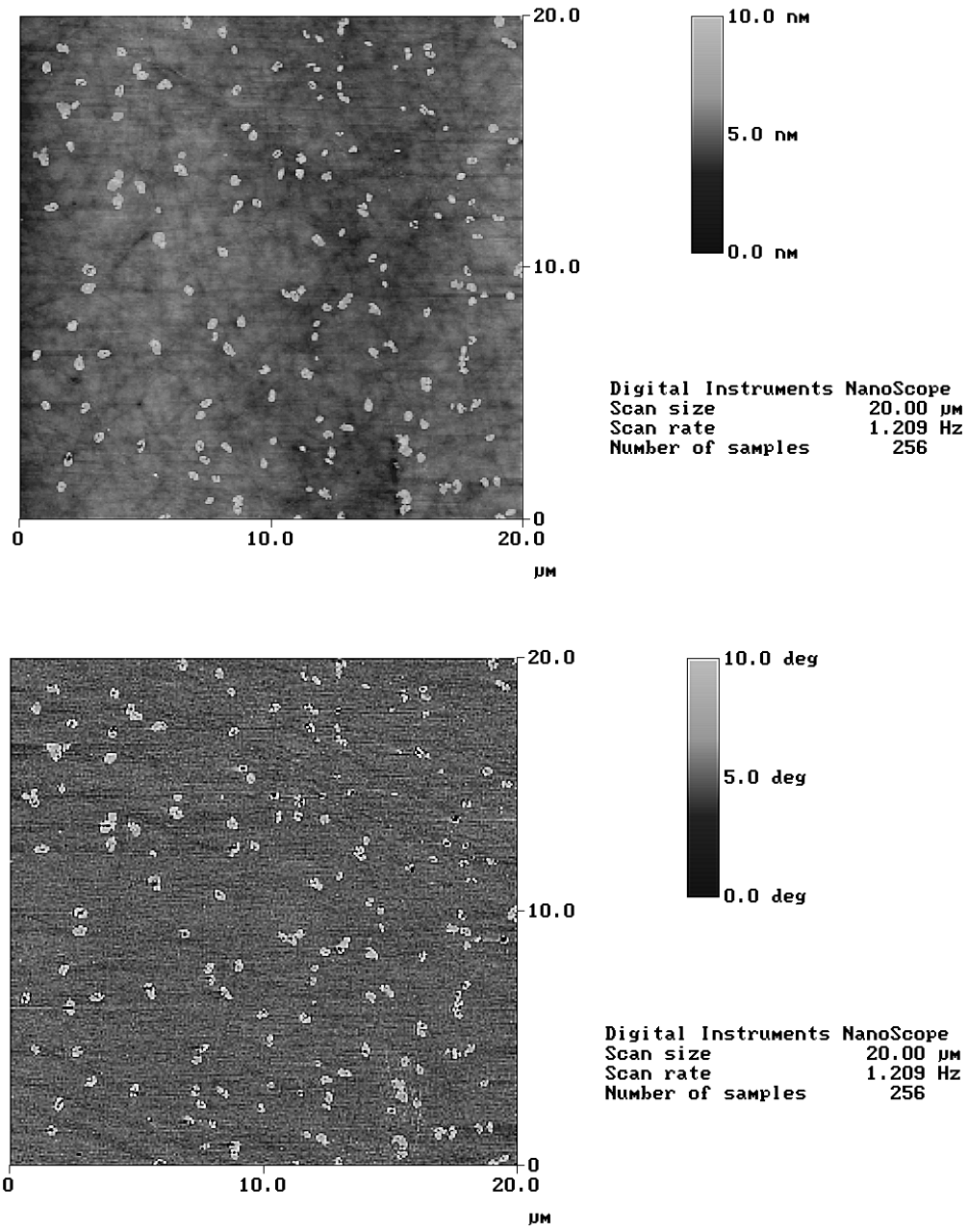

Figure 5–8. Topographical information (top); the same area (bottom) in phase imaging mode

An XPS survey scan (§5.6) of this area yields little extra information on the nature of these particulates. The only contaminants identified on the surface were carbon and oxygen. It is possible that other contaminants may exist on the surface that are below the threshold of detection of XPS but this technique is highly sensitive.

5.9.2.2 Cleaning the surface

An ideal cleaning process has three outcomes: 1) effective removal of contaminants; 2) no physical damage to the surface; and 3) reproducibility. Reproducibility may be best achieved using a process that is not reliant on manual handling. A further consideration may be the chemical state of the cleaned surface. For example, one may be concerned with the hydrophilicity of the cleaned surface.

Two organic solvents, isopropyl alcohol and acetone, were used in a first attempt at removing the observed structures. Firstly, by immersion of the surface for several hours in each of the solvents. Secondly, by use with an ultrasonic cleaning bath to increase the mechanical energy of the process. Neither technique and neither solvent were effective at removing these contaminants. The next stage was to use a technique used at the Bureau International des Poids et Mesures (BIPM) for the routine cleaning of mass standards manufactured from stainless steel and platinum-iridium. This method uses a 50:50 solution of ether and ethanol, which is applied manually using a lens cloth with a relatively firm pressure. This proved to be very effective at removing both types of contaminant from the silicon surfaces. Being a manual process, the reproducibility is very much dependent on the operator but it was decided to use this technique to clean the cylindrical artefacts being used in the mass stability investigation. The surface is left hydrophobic.

5.9.3 Cylindrical samples

Figure 5–9 shows an AFM scan on the side of a cylindrical artefact that had been manufactured and polished at NPL (§2.3.2). Structure due to the non-random nature of the polishing process can clearly be seen. A series of radial grooves run around the side of the cylinder. Several scratches can be seen in the top left corner of the image and generally there is a noticeable increase in the level of pitting compared with the flat surfaces. This is evidence that insufficient material was removed during one or more of the polishing stages and damage from a previous stage still exists within the crystal.

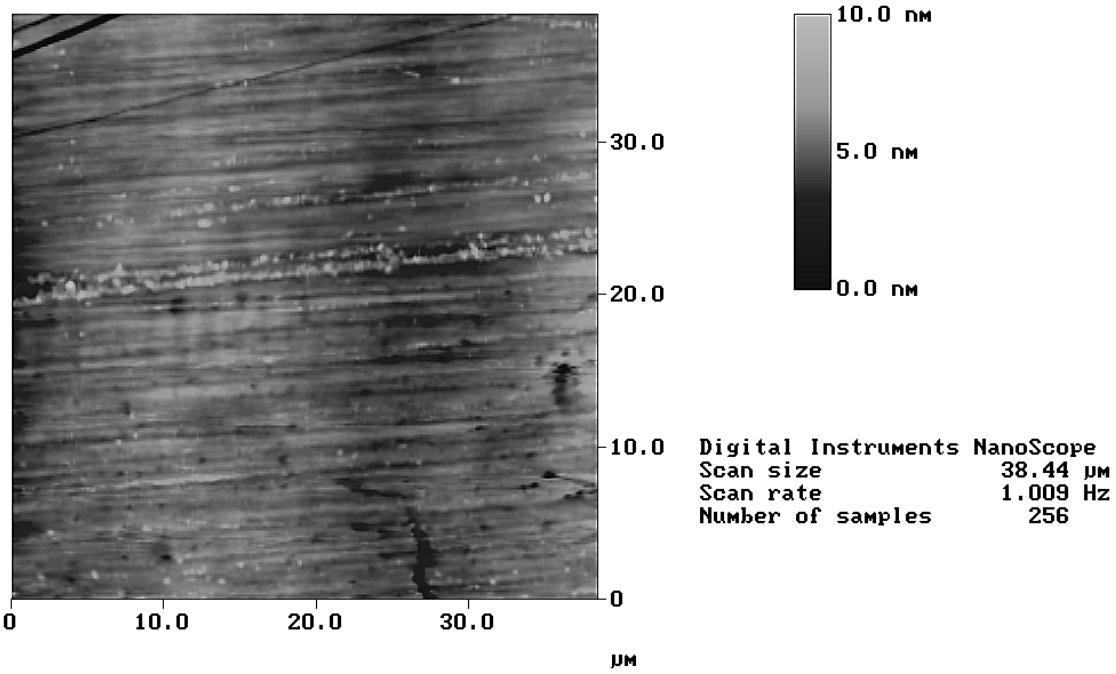

Figure 5–9. Side of a cylindrical artefact showing radial structure due to polishing process

A cross sectional analysis of this image reveals a series of grooves with widths in the range 1 to 2 µm and height of around 2 nm, with finer grooves superimposed on this structure. Typical values of *Ra* for this surface were of the order 0.5 nm.

6 FURTHER PLANNED EXPERIMENTAL STAGES

6.1 Surface study objectives

The scientific objectives of surface study work at NPL have been stated at §(1.3). This Section describes the planned experimental stages that are required to meet these objectives.

6.2 Carbonaceous layer

6.2.1 Composition of carbonaceous layer

High resolution XPS scans of the carbon peak will be obtained for silicon surfaces. The data will be fitted to determine the relative contributions of the four functional groups (§5.6) for silicon surfaces which have been polished at NPL and kept in appropriate storage conditions.

6.2.2 Optical constants of carbonaceous layer

Having determined the composition of the carbon peak, the next task will be to identify a substance that best matches this profile. The optical constants of this substance will then be used in the ellipsometry model. The validity of the model to determine layer thickness will be directly checked against the XPS data.

6.3 Oxide layer

6.3.1 XPS and RBS measurements

Generally, the agreement between these two techniques was reasonable (§5.5.1). However, there were several instances when there was a large discrepancy in the measurement of the thickness of an oxide layer. It is vital to understand all the contributions to the uncertainty for both of these techniques and the impact of any assumptions that have been made. In particular, the relative amount of oxygen within the oxide and carbonaceous layer needs to be determined. This will establish the stoichiometry and enable corrections to be applied to the RBS result. A silicon wafer with a well defined stoichiometric oxide should also be

quantified using the instruments involved. XPS analysis needs the most accurate values of attenuation length λ_f.

6.3.2 Repeat process on new set of wafers

The polishing and measurement procedure will be repeated for a new set of wafers with differing orientations. These experiments will yield further information on the agreement between the techniques as well as information on the reproducibility of the polishing process.

6.3.3 Stoichiometry of native oxide

Again, it is vital to understand and quantify all the contributions to the XPS measurement uncertainty. This will include making a correction to the measured oxide peaks for an overlayer of adventitious carbon [17]. The instrument's sensitivities to oxygen and silicon also needs to be established. Having made these advances, angle resolved XPS will be used to establish a depth profile of the oxygen signal.

6.3.4 Optical constants of native oxide

Reliable values of optical constants will enable more accurate determination of oxide thickness via ellipsometry. Previous data will be re-modelled using the oxide thickness as determined by XPS/RBS as an input parameter. It is intended that a consistent set of values can be applied to all surfaces polished in this manner.

6.4 Amorphous layer

6.4.1 Transmission electron microscopy

The underlying surface structure will be investigated using High Resolution Transmission Electron Microscopy (HTEM). This may provide the resolution to help validate the thickness

of amorphous layers measured by RBS. Sample preparation can, however, potentially alter the oxide thickness [28]

6.4.2 Optical constants of amorphous layer

In common with the method to determine the optical constants of the oxide, the RBS measurement of the thickness of amorphous layers will be used, via VASE modelling, to determine the optical constants for this type of structure. It may be found that the optical constants of the amorphous silicon show an orientation dependence.

6.5 Measurements on silicon spheres

6.5.1 Crystallographic orientation of spheres

An experimental silicon sphere has been manufactured at NPL. By June 2001 a second sphere will be completed. Prior to their surface analyses, the artefacts' crystallographic orientations have to be determined and identified. X-ray diffraction is routinely used for orientating single crystals both in academic and industrial environments. However, most apparatus are used with goniometers that are restricted to relatively small samples. To this end, an experiment will be set-up using facilities and expertise at the Royal Holloway College (University of London), to determine the crystallographic orientation of the silicon spheres used in this project.

6.5.2 Ellipsometry on spheres

Having developed the optical models used by the ellipsometer, the technique will then be used to determine the thickness of contaminating layers on the two NPL silicon spheres. Measurements will use the focused beam attachment and a goniometer on the instrument's translation stage. In this manner, damage to the surface and growth of the oxide can be directly quantified against the crystallographic orientation. Having access to two spheres will enable the reproducibility of the polishing process to be established. To confirm the validity of these measurements, the surface of one sphere will be dissected and samples analysed

using RBS and XPS. These samples will also be used to investigate the long-term stability of the oxide and carbonaceous layers.

The results of this work can be compared with the results published by CSIRO [3] obtained using an ellipsometer and relying upon optical constants based on bulk silicon dioxide and an evaporated film (§4.2.5).

6.5.3 Surface texture of spheres

Measurements of the surface texture have been made using the Nanoscope III instrument (§4.5.2). The physical size of a sample that can be mounted in this instrument is restricted to around 1 x 1 x 0.5 cm. The University of Surrey owns a second instrument, manufactured by NT-MDT Molecular Devices and Tools for NanoTechnology, which can be used with large samples. However, it will require development work for use with very smooth, highly reflecting samples such as NPL polished silicon surfaces.

6.6 Surface preparation and growth of a thermal oxide

Finally, the remaining uncut sphere (§6.5.2) will be treated, possibly using an RCA clean with an etching stage to remove the native oxide, and a thermal oxide grown on the surface. This will be a one-off experiment to determine if a relatively straightforward procedure, common place in the semiconductor industries, can be transferred to a sphere to grow a thin, stoichiometric oxide layer. The possibility of using facilities at a semiconductor fabrication plant will be investigated.

7 ACKNOWLEDGEMENTS

The author would like to thank: Dr J Keddie, Prof K Puttick, Dr P Zhdan, Dr C Jeynes and Prof J Watts of the University of Surrey; Dr E Wendler of the University of Jena; Dr R Leach of the National Physical Laboratory. The work for this report was funded by the Department of Trade and Industry, National Measurement System Policy Unit, under the National Measurement System Mass Programme, 1999-2002.

8 REFERENCES

[1] Downes, S.P. Present status of the different approaches to the re-definition of the kilogram. *NPL Report CMAM 11*, 1998.

[2] Zarudi, I. and Zhang, L. Subsurface damage in single-crystal silicon due to grinding and polishing. *Journal of Materials Science Letters*, 1996, **15**, 586-587.

[3] Kenny, M.J. *et. al*. Surface layer impurities on silicon spheres used in determination of the Avogadro constant. *IEEE Transactions on Instrumentation and Measurement*, April 1999, **48**, (2), 233-237.

[4] Fujii, K. *et. al*. Determination of the Avogadro constant by accurate measurement of the molar volume of a silicon crystal. *Metrologia*, 1999, **36**, 455-464.

[5] Leistner, A.J and Giardini, W.J. Fabrication and sphericity measurements of single-crystal silicon spheres. *Metrologia*, 1994, **31**, 231-243.

[6] Whitmore, L.C. Microscopy of nano-machined silicon. *Thesis*, December 1994, University of Surrey.

[7] Johansson, S and Schweitz, J. Surface defects in polished silicon studied by cross-sectional transmission electron microscopy. *J. Am. Ceram. Soc*., 1989, **72, (**7), 1136-1139.

[8] Joyce, B.A and Neave, J.H. *Surface Sci*.,1971, **27**, 499.

[9] Sze, S.M. *Semiconductor devices, physics and technology*. USA, Wiley, 1985.

[10] Gonda, S. *et. al*. Sub-nanometer scale measurements of silicon oxide thickness by spectroscopic ellipsometry. Jpn. J. Appl. Phys., 1998, **37**, L1418-L1420

[11] Azzam, R.M.A and Bashara, N.M. *Ellipsometry and polarised light*. Amsterdam, North Holland, 1987.

[12] Styrkas, D. *et. al*. *Application of ellipsometry to polymers at interfaces and in thin films*. Polymer Surfaces and Interfaces III, John Wiley and Sons Ltd, 1999.

[13] Guide to using WVASE32, J.A. Woollam Co., Inc.

[14] Palik, E. *Handbook of optical constants of solids*. Academic Press, 1985.

[15] Earwaker, L.G. Rutherford backscattering and nuclear reaction analysis. *Vacuum*, 1994, **45**, (6-7), 783-803.

[16] Watts, J. F. *An introduction to surface analysis by electron spectroscopy*. Microscopy Handbooks **22**, Oxford University Press, 1990.

[17] Mitchell, D.F *et. al*. Film thickness measurement of SiO2 by XPS. *Surf. Interface Anal.*, 1994, **21**, 44-50.

[18] Cumpson, P. Estimation of inelastic mean free paths for polymers and other organic materials: use of quantitative structure-property relationships. *Surf. Interface Anal.*, 2001, **31**, 23-34.

[19] Wiesendanger, R.W. *Scanning probe microscopy and spectroscopy – methods and applications*. Cambridge University Press, 1994

[20] Binnig, G and Quate, C.F. Atomic Force Microscope. *Phys. Rev. Lett*., 1986, **56(9)**, 930-933.

[21] Kern, W. and Puotinen, D. Cleaning solutions based on hydrogen peroxide for use in silicon semiconductor technology. *RCA Review*, 1970, **June**, 187-206.

[22] Fair, R.B. J. Electrochem. Soc., 1981, **128**, 1360.

[23] Danzebrink, H.U. *et. al*. Ellipsometric measurements on single-crystal silicon spheres. To be published in proceedings of CPEM 2000, Sydney, Australia.

[24] Gross, T. *et. al.* Uncertainty in measurement of overlayer thickness of thermally oxidised silicon using x-ray photoelectron spectroscopy. *Surf. Interface Anal*., 2000, **29**, 891-894.

[25] Iler, R.K. *The chemistry of silica. solubility, polymerization, colloid and surface properties and biochemistry*. Wiley, 1979.

[26] Raider, S.I. *et. al.* Oxide growth on etched silicon in air at room temperature. *J. Electrochem. Soc: solid-state science and technology*, 1975, **122**, 3, 413-418.

[27] Cumpson, P.J and Seah, M.P. Stability of reference masses IV: growth of carbonaceous contamination on platinum-iridium alloy surfaces, and cleaning by UV/ozone treatment. *Metrologia*, 1996, **33**, 507-532.

[28] Vanhellemont, J. *et al*. Round robin investigation of silicon oxide on silicon reference materials for ellipsometry. *Applied Surface Science*, 1993, **63**, 45-51.

9 APPENDIX 1: PRINCIPLES OF ELLIPSOMETRY

9.1 Ellipsometric angles

Ellipsometry measures the change in the polarisation state of a light beam that has been reflected from or transmitted through the sample under study. Ellipsometry derives its name from the fact that it analyses the polarisation of elliptically polarised light in order to determine its ellipticity [11]. The principles of operation are shown in Figure 4–1. A light beam with a known initial polarisation (usually linear) is reflected from a sample causing the light to become elliptically polarised. The change in amplitude and phase of polarisation can be determined by resolving the electric vector into two components: parallel (*p*) to and perpendicular (*s*) to the plane of incidence, which is defined as the plane containing the incident and reflected beams and the vector normal to the sample surface.

Two ellipsometric angles known as Ψ and Δ may be defined. Prior to reflection, the polarisation of light is determined by the amplitude ratio A_p/A_s, and the phase difference δ_p-δ_s, of the two components *p* and *s*. Upon reflection, both the amplitude ratio and the phase difference change. The angle Δ is the change in phase difference caused by the reflection and is given by:

Equation 9–1

$$\Delta = \left(\delta_p - \delta_s\right)_{reflected} - \left(\delta_p - \delta_s\right)_{incident}$$

The angle Ψ is defined by the ratio of the amplitude ratios before and after reflection and is given by:

Equation 9–2

$$\Psi = \left(\frac{\left(A_p \,/\, A_s\right)_{reflected}}{\left(A_p \,/\, A_s\right)_{incident}} \right)$$

If the incident beam is linearly polarised, the above equations can be simplified. Linearly polarised light can be described as two orthogonal electric fields propagating in phase. There is no initial phase difference between the *p* and *s* components and Equation 9–1 simplifies to:

Equation 9–3

$$\Delta = \left(\delta_p - \delta_s\right)_{reflected}$$

The ellipsometric angle Ψ is defined by Equation 9–2 since the *p* and *s* components can have any magnitude and ratio, depending on the incident light intensity and the position of the polariser.

9.2 Reflection coefficients

The measured angles Ψ and Δ can be related to the optical constants and dimensions of a sample via the Fresnel reflection coefficients R_p and R_s. The ratio of these coefficients defines the ellipticity ρ, which is a complex number. This ratio is mathematically related to the two ellipsometric angles Ψ and Δ through the equation of ellipticity:

Equation 9–4

$$\rho = \frac{R_p}{R_s} = \tan\left(\Psi\right) e^{i\Delta}$$

9.2.1 Reflection at a planar interface

The propagation of a plane wave in an isotropic absorbing medium is described by the complex refractive index *N* which consists of a *real component* (*n*, refractive index) and *imaginary component* (*k*, extinction coefficient) and can be written:

Equation 9–5

$$N = n - jk$$

The refractive index n determines how fast the phase of a propagating wave changes and the extinction coefficient k determines how fast the amplitude of a propagating wave decreases. For non-absorbing i.e. transparent materials the extinction coefficient goes to zero (k=0). At a planar interface between two mediums, the Fresnel reflection coefficients are related to the complex refractive indices, N_1 and N_2 of the mediums as follows:

Equation 9–6

$$R_p = \frac{N_2 \cos\theta_i - N_1 \cos\theta_r}{N_2 \cos\theta_i + N_1 \cos\theta_r}$$

and

Equation 9–7

$$R_s = \frac{N_1 \cos\theta_i - N_2 \cos\theta_r}{N_1 \cos\theta_i + N_2 \cos\theta_r}$$

where θ_i is the angle of incidence (measured from the sample normal) and θ_r is the angle of refraction. If we substitute for R_p and R_s in Equation 9–4 and make use of Snell's law ($N_1 sin\theta_i = N_2 sin\theta_r$) we have:

Equation 9–8

$$N_2 = N_1 \tan\theta_i \left[1 - \frac{4\rho}{(1+\rho)^2} \sin^2\theta_i \right]^{1/2}$$

Hence, the complex refractive index of medium 2 can be determined from a knowledge of the refractive index of medium 1 and the measurement of ellipticity ρ at one angle of incidence. If medium 1 is air then N_1=1. As can be seen from Equation 9–4, Equation 9–6 and Equation 9–7 the ellipsometric angles Ψ and Δ are a function of the refractive index of the two mediums at the interface. By implication they are also dependent on the wavelength of light, since the refractive index is dependent on the wavelength of light.

9.2.2 Reflection and transmission by an ambient-film-substrate system

An important application of ellipsometry is the measurement of the thickness of films and coatings. Consider the physical model shown by Figure 9–1. Here the film has parallel-plane boundaries (i.e. 'slab' model) with a separation of d_1 and is sandwiched between an ambient and substrate medium.

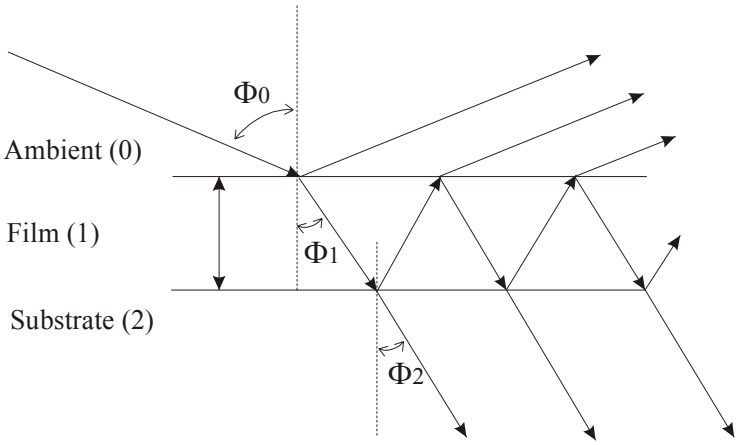

Figure 9–1: Oblique reflection and transmission of a plane wave by an ambient(0)–film-(1)-substrate(2) system with parallel-lane boundaries

All three mediums are homogenous and optically isotropic, with complex refractive indices of N_0, N_1 and N_2 respectively. If the ambient medium is transparent then N_0 is real. The Fresnel coefficients describing this optical system are then modified with an exponential term containing a parameter β defined by:

Equation 9–9

$$\beta = 2\pi\, N_1 \frac{d_1}{\lambda} \cos\theta_i$$

where β is the phase angle or *film phase thickness* and is defined as the phase change that the multiply-reflected wave inside the film experiences as is traverses the film once from one boundary to the other. Thus, if the refractive index of the film N_1 is known, its thickness can be determined from at least one measurement at a given wavelength and angle of incidence.

10 APPENDIX 2: CHARACTERISATION OF A FOCUSING UNIT FOR THE MEASUREMENT OF OXIDE THICKNESS ON SILICON ARTEFACTS BY ELLIPSOMETRY

10.1 Introduction

The diameter of the light beam used by the Variable Angle Spectroscopic Ellipsometer (VASE) in its standard configuration is approximately 2.5 mm. This is adequate when determining the thickness or optical constants of thin films on flat substrates and when an 'average' of the measured parameters over a relatively large area is permissible. At a typical angle-of-incidence of 75° (measured with respect to the surface normal) the area covered by the beam on a sample's surface is approximately 25 mm^2. When the area of interest is much smaller or the sample has a curved surface, a means of focusing or reducing the beam size is required.

10.2 Surface geometry and beam diameter

The Avogadro project at the National Physical Laboratory (NPL) utilises artefacts manufactured from silicon single crystal which can be cylindrical (with a diameter of approximately 60 mm) or spherical (with a diameter of approximately 90 mm) in form. In these circumstances, the beam diameter is too large; the curvature of the surface causes excessive divergence of the reflected beam resulting in a poor signal-to-noise ratio at the detector. Figure 10–1 and Figure 10–2 show typical results for the two measured ellipsometric angles, psi Ψ and delta Δ, obtained for a flat and cylindrical artefact respectively, using the unmodified optics. In the latter case, the signal to noise ratio at the detector is greatly reduced leading to data which cannot be reliably modelled. Modelling the experimental data in this example led to an overestimation of the oxide thickness by approximately 70 %.

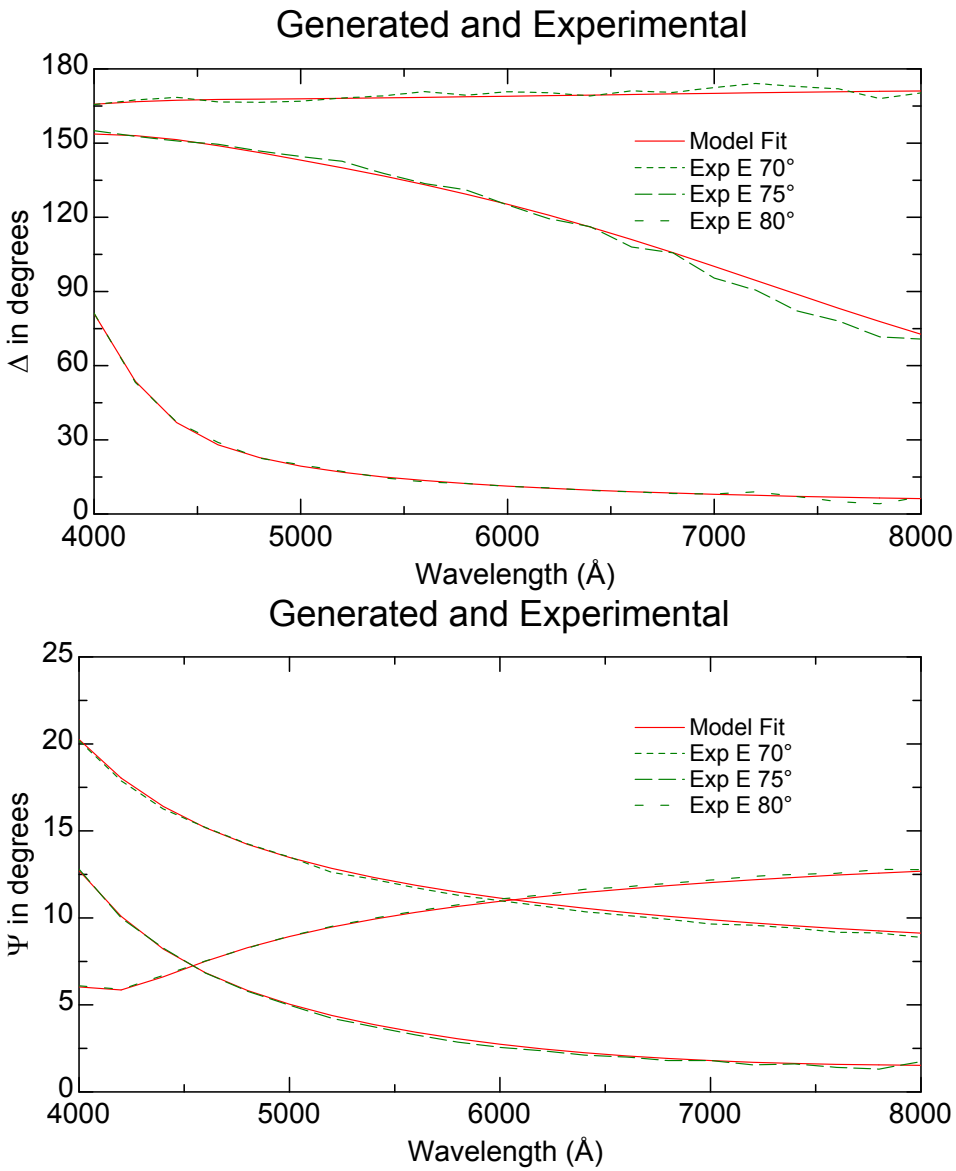

Figure 10–1. Measured ellipsometric angles on a flat surface. The fitted data gave an oxide thickness of 34 Å

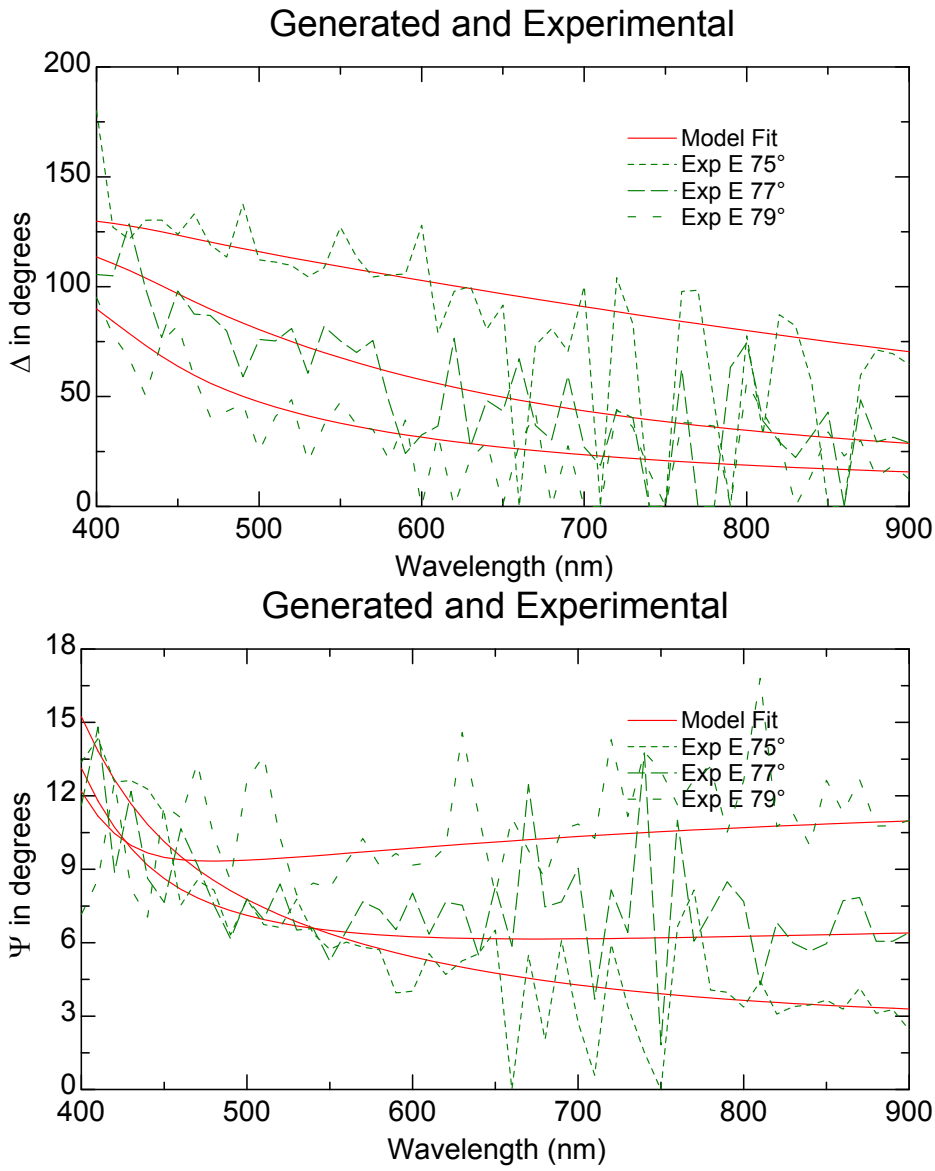

Figure 10–2. Measured ellipsometric angles on the side of a cylinder (nominal diameter 60 mm). The fitted data gave an oxide thickness of 86 Å

10.3 Focusing unit

A pair of focusing probes specifically manufactured for the VASE were obtained from J.A. Woollam Co. Figure 10–3 shows the probes prior to their installation and in use on the ellipsometer.

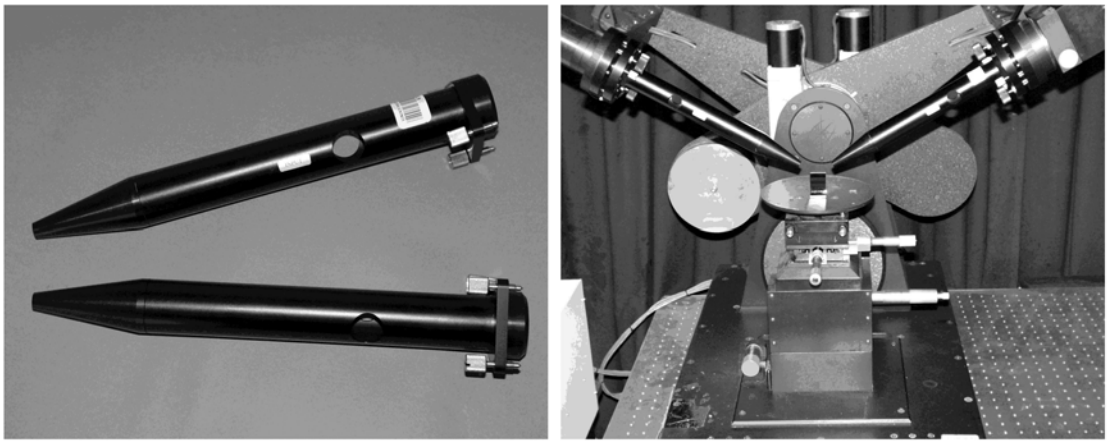

Figure 10–3. Focus probes used with the VASE ellipsometer

The two probes are identical in construction and consist of a hollow tube (provided with screws and adjustable mounts for attachment to the VASE and optical alignment) which has a small focusing lens at one end. This has a focal length of approximately 30 mm. The beam size is reduced to approximately 0.2 mm when focused onto a sample. However, a consequence of using such a device is the convergence and then the divergence of the beam from the surface. The general equations of ellipsometry are derived for parallel light rays [11]Any departure from this condition will lead to an error when determining a film's thickness. Fortunately, the VASE software [13] has a feature to compensate for this effect and a value can be entered for the 'angular spread' of the beam. The angular spread is effectively half of the solid angle (approximately 5°) formed by the beam at the surface of the sample (as illustrated in Figure 10–4) and is dependent on the diameter of the beam emerging from the polariser and on the focal length of the probes.

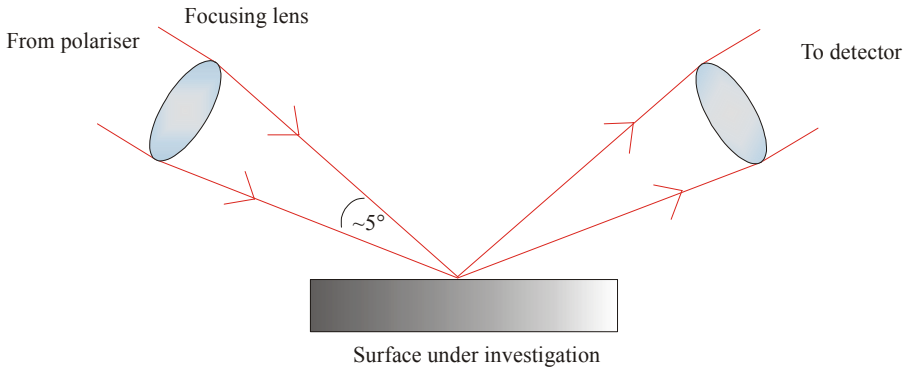

Figure 10–4. Convergence and then divergence of the light beam reflected from a surface

10.4 Determining the angular spread

10.4.1 Modelling strategies

The angular spread will depend on the beam diameter and focal length of the probes, which leads to a unique value for each instrument and probe combination. The angular spread was determined by comparing measurements made using the standard optics with those with the focusing probes. For the purposes of this work it is assumed that the conventional optics provides an accurate measurement of oxide thickness and any deviation is presumed to result from errors introduced by the focusing probes.

Three flat wafers were chosen for this study. Each has been manufactured from silicon single crystal and polished on one side, with nominal oxide thicknesses of 30 Å, 160 Å and 260 Å. The 30 Å and 160 Å wafers effectively bracket the range of thicknesses likely to be encountered for artefacts used in the Avogadro project; the 260 Å wafer was included to provide more information on the modelling process. The wafers were supplied as <100> orientation. Although their precise oxide stoichiometry is not known, a simple model assuming an SiO_2 layer on a silicon substrate should suffice. An error in the model will give rise to the same systematic error in both optical configurations. Furthermore, we are not interested here in the absolute accuracy of a given measurement but rather the differences between the two configurations.

Two approaches to modelling the experimental results with the focusing probes were used: 1) both the thickness and the angular spread were chosen as fit parameters; and 2) the model assumed the thickness to be that measured by the standard optics and a fit of only the angular spread was made. Table 1 gives a summary of the results obtained from four or five independent trials for each wafer. The mean squared error (MSE) is the sum of the squares of the differences between each calculated (modelled) and experimental data point, divided by the standard deviation of the experimental data point. When the MSE is unity or less, the calculated data lie within one standard deviation of the experimental data.

	Standard Optics		Focusing Unit												
	Model:Si/SiO2		Model:Si/SiO2			Model:Si/SiO2+spread				Model:Si/SiO2+spread			Model:Si/SiO2+spread+angle	
Date	Fit:thickness		Fit:thickness			Fit:thickness+spread				Fit:spread			Fit:spread+angle	
	Thickness	MSE	Thickness	MSE	Absolute difference	Thickness	Spread	MSE	Absolute difference	Thickness	Spread	MSE	Spread	MSE
	Å		Å		Å	Å	°		Å	Å	°		°	
17-May	28.75	2.48	35.02	3.94	6.27	26.76	2.38	3.11	1.99	28.75	2.15	3.15	2.14	1.99
17-May	29.44	2.46	36.80	3.76	7.36	28.31	2.23	2.77	1.13	29.44	2.11	2.78	2.11	2.57
19-May	29.67	2.74	37.97	4.66	8.30	27.52	2.50	3.33	2.15	29.67	2.29	3.37	2.24	2.48
25-May	29.15	2.59	37.70	6.15	8.55	24.28	2.78	4.87	4.87	29.15	2.37	5.00	2.19	2.29
Average	29.25	2.57	36.87	4.63	7.62	26.72	2.47	3.52	2.54	29.25	2.23	3.58	2.17	2.33
Std dev.	0.40		1.33			1.74	0.23			0.40	0.12		0.06	
17-May	162.18	2.56	164.42	3.91	2.24	163.37	1.72	3.90	1.19	162.18	2.34	3.91	1.34	1.86
17-May	162.29	2.55	163.71	2.55	1.42	162.75	1.69	2.52	0.46	162.29	1.99	2.52	1.79	1.83
19-May	162.85	2.61	166.12	3.36	3.27	163.90	2.60	3.24	1.05	162.85	3.05	3.26	2.53	1.93
19-May	162.85	2.69	164.02	2.22	1.17	163.89	0.62	2.22	1.04	162.85	1.72	2.25	2.08	1.93
25-May	163.08	2.32	165.43	2.31	2.35	163.66	2.24	2.19	0.58	163.08	2.50	2.19	2.27	1.90
Average	162.65	2.55	164.74	2.87	2.09	163.51	1.77	2.81	0.86	162.65	2.32	2.83	2.00	1.89
Std dev.	0.39		1.01			0.48	0.75			0.39	0.51		0.46	
17-May	262.73	2.70	264.58	3.08	1.85	261.72	3.23	2.91	1.01	262.73	2.70	2.93	1.27	1.72
17-May	261.86	2.69	260.87	2.36	0.99	260.87	0.00	2.37	0.99	261.86	0.00	2.54	0.00	1.75
19-May	263.98	2.89	266.20	4.04	2.22	262.88	3.49	3.85	1.10	263.98	2.95	3.86	0.74	1.69
25-May	272.47	2.62	267.44	3.26	5.03	263.36	3.93	3.07	9.11	272.47	0.00	4.69	0.00	4.63
25-May	266.41	2.59	274.44	3.14	8.03	271.74	3.17	3.02	5.33	266.41	5.19	3.41	4.58	2.49
Average	265.49	2.70	266.71	3.18	3.62	264.11	2.76	3.04	1.38	265.49	2.17	3.49	1.32	2.46
Std dev.	4.26		4.98			4.37	1.57			4.26	2.20		1.90	

Table 10-1. Summary of calculated oxide thickness and angular spread

10.4.2 Observations

10.4.2.1 Error due to beam focusing

For all three wafers, the result of not fitting for angular spread gave rise to an average oxide thickness that was higher than that obtained with the standard optics in place. The over estimation was approximately 26 % for the 30 Å wafer and 1 % for the 160 Å and 260 Å wafers respectively. In the latter two cases, the change in the measured parameters Ψ and Δ between the two optical configurations was small and led to a corresponding higher degree of uncertainty when fitting the data for angular spread. This is demonstrated by the higher standard deviations when calculating the mean value. For this reason the final calculation of

the angular spread has been based solely on the results obtained for the 30 Å wafer. Figure 10–5 and Figure 10–6 demonstrate the effects of the focusing probes by showing the change in the measured parameters for the 30 Å and 160 Å wafers.

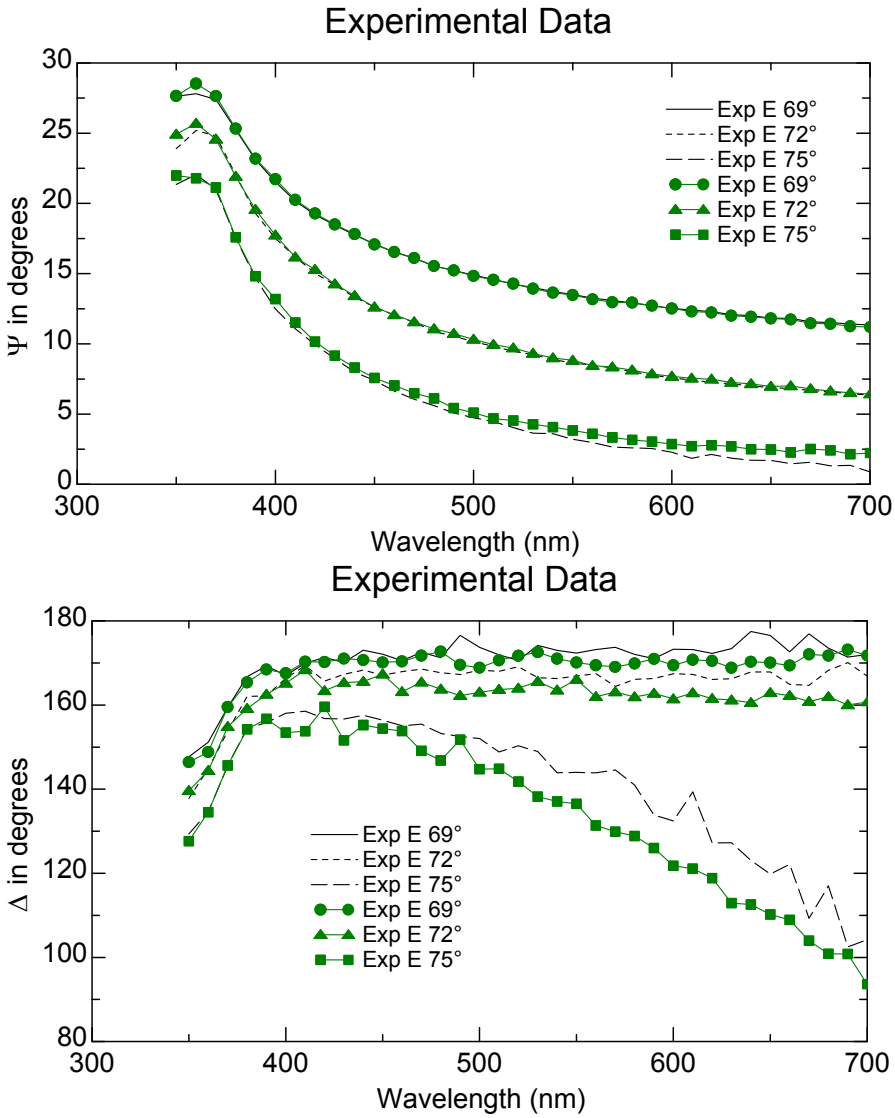

Figure 10–5. Measured ellipsometric angles using the standard configuration (lines) and focusing probes (data points) for the 30 Å wafer

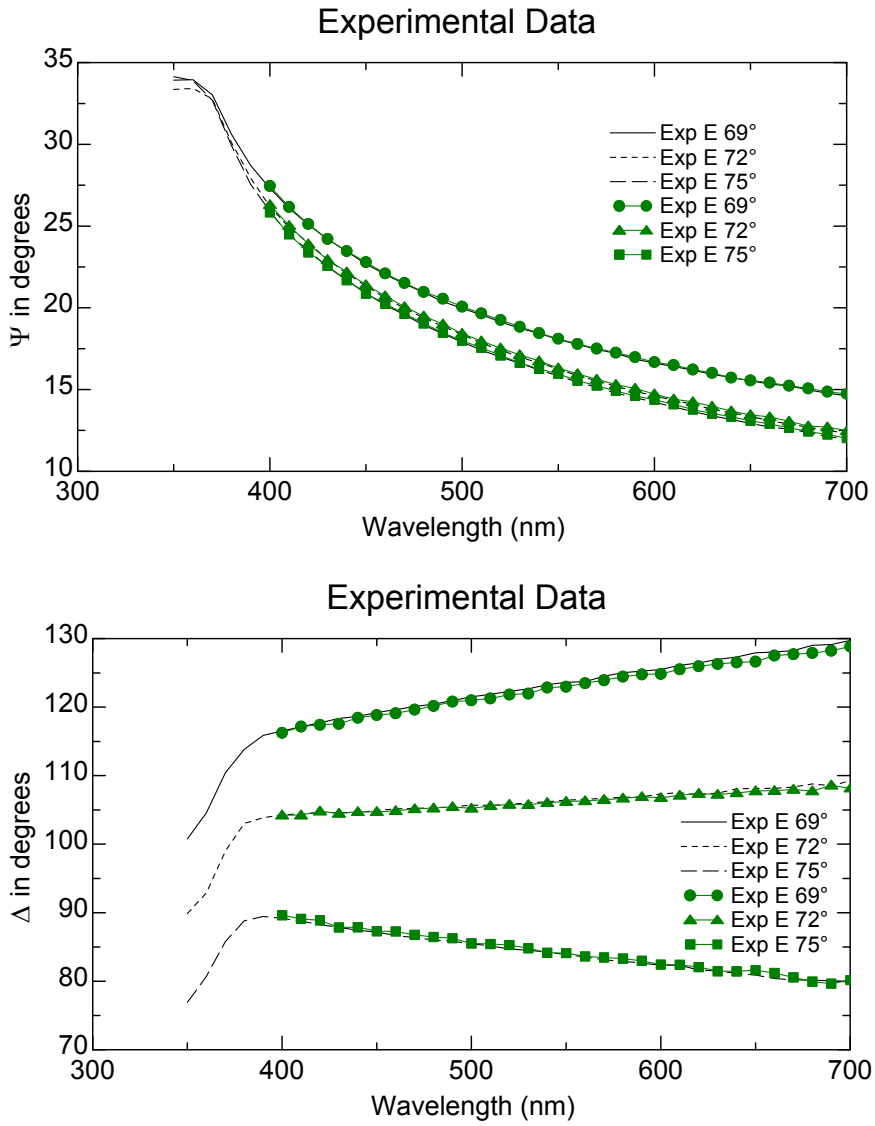

Figure 10–6. Measured ellipsometric angles using the standard configuration (lines) and focusing probes (data points) for the 160 Å wafer

10.4.2.2 Correlation

Both approaches to modelling (§10.4.1) yielded similar results for the angular spread. However, in approach (1) there was a strong correlation[7] between the two fit parameters (thickness and angular spread). For this reason approach (2) was used for the measurement of the angular spread. In most cases, this model was further improved by fitting for the angle of the incident beam measured with respect to the surface normal. The deviation from the nominal value is probably due to a slight misalignment of the focusing lens in either or both of the probes with respect to the beam.

10.4.2.3 Estimation of angular spread

For the reasons stated above, the angular spread of this beam/probe combination has been estimated from the results obtained with the 30 Å wafer. The thickness of the oxide has been measured using the standard optics. The angular spread and angle-of-incidence have been used as fit parameters. In total, four measurements of the angular spread were made giving a mean value of 2.17° with a standard deviation of ± 0.06°. Figure 10–7 gives an example of the fit obtained for one of these measurements.

[7] The VASE software is capable of displaying a 'correlation matrix' for any two parameters used in the fitting process. The components of this matrix are derived from the covariances of the calculated best-fit and describe the degree of independence of the two parameters.

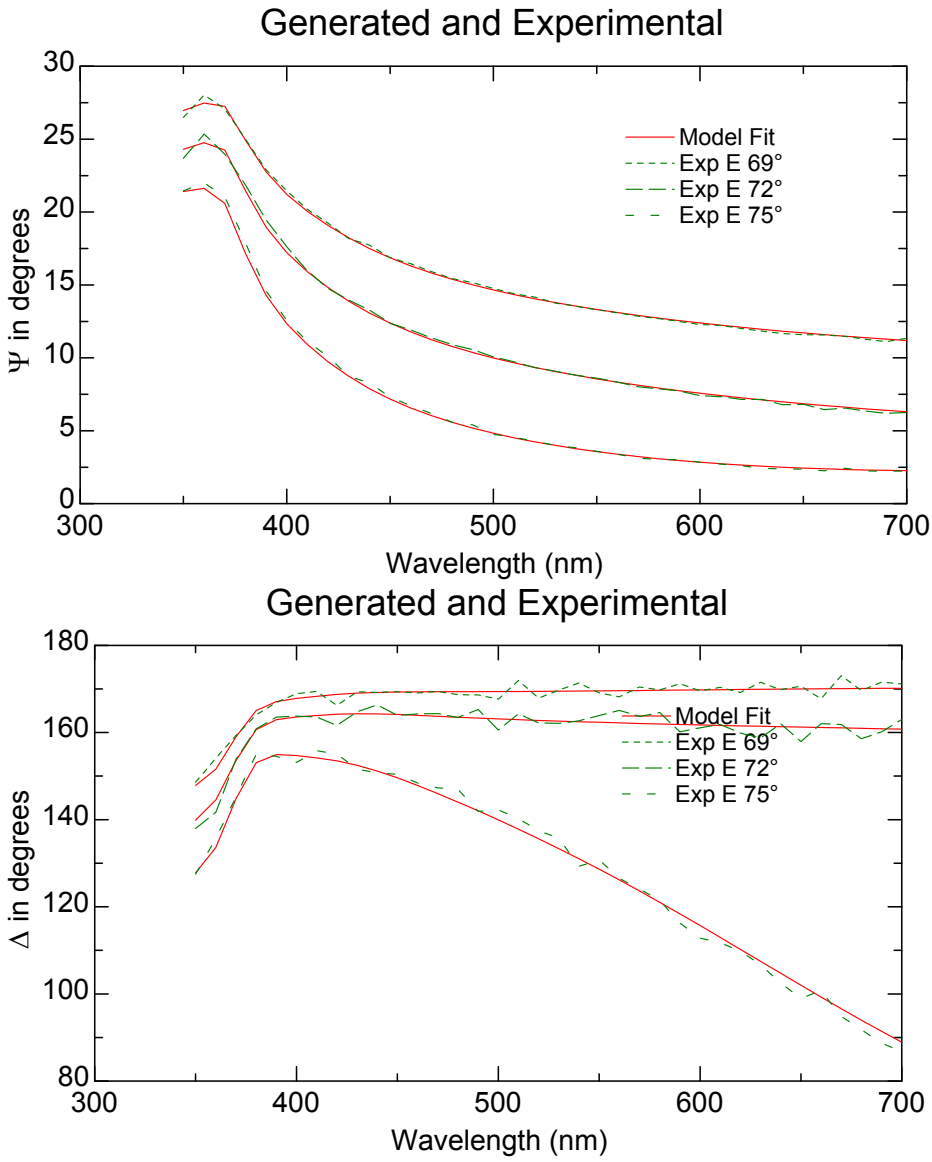

Figure 10–7. Measured ellipsometric angles and modelled fit for 30 Å wafer

10.5 Measurements made on a cylindrical artefact

10.5.1 Experimental procedure

Measurements were made on a cylindrical artefact to test the quality of the fit obtained when modelling with an angular spread of 2.2°. The artefact has an approximate diameter of 60 mm and has been cut in two, through its axis of symmetry, to facilitate easy mounting on the translation stage of the ellipsometer. The cylindrical axis has been orientated in-line with the incident beam as shown by Figure 10–8.

Figure 10–8. Artefact mounted on the ellipsometer's translation stage

A single measurement consisted of a spectroscopic scan over the wavelength range from 350 nm to 700 nm, at nominal angles of incidence of 69°, 72° and 75°. The alignment procedure consisted of the following stages: 1) alignment of the artefact using the standard optics; and 2) alignment of probes with respect to the polariser and detector using the supplied mounting screws. Stage (2) usually involves an iterative process to ensure correct alignment. Table 10-2 shows the results of these measurements.

	Model:Si/SiO2+spread (2.2°) Fit:thickness		Model:Si/SiO2+spread (2.2°) Fit:thickness+angle		
Date	Thickness Å	MSE	Thickness Å	MSE	Angle °
16-Feb-00	50.60	9.11	51.39	1.86	69.42 ± 0.016 72.34 ± 0.015 75.23 ± 0.009
16-Feb-00	48.94	4.37	49.70	1.73	69.22 ± 0.015 72.16 ± 0.014 75.07 ± 0.008

Table 10-2. Calculation of oxide thickness and angle of incidence for measurements made on the cylindrical artefact

10.5.2 Observations

10.5.2.1 Model

In common with the measurements made on the flat wafers, a convincing model was only obtained when the angle-of-incidence was also used as a fit parameter. This led to a large reduction in the MSE values but the corresponding change in the thickness was less than 1 Å. An angular spread of 2.2° was assumed and thickness and angle-of-incidence were used as the fit parameters. However, the departure of the angles from their nominal values (69°, 72° and 75°) was more pronounced than that obtained with the flat wafers (typically 0.1°). This is probably due to the difficulties in aligning the artefact in the first place, as well as any misalignment of the lenses. The standard optics are used to align the artefact with respect to the beam and the task is made significantly harder due to the divergence of the beam after reflection from a curved surface. There would appear to be a bias to this procedure as the fitted angles tend to be less than nominal.

10.5.2.2 Varying the angle-of-incidence

To test the assumption that the artefact was misaligned, the artefact was deliberately tilted with respect to the beam using the levelling screws on the translation stage of the VASE. Table 10-3 gives a summary of the measurements. The column headed ‘tilt position’ is an arbitrary scale and represents the fraction by which the levelling screw is rotated (i.e. 0.500 = 180°); the position 0 represents the initial setting of the screw when the artefact is first aligned. A positive value represents a decrease in the angle-of-incidence, a negative value an increase. The data highlighted (*italics*) indicate a ‘zero point’ where the fit and nominal angles best agree.

The assumption appears robust with the predicted variation in the calculation of the angle-of-incidence with tilt. A good level of fit was obtained, and the thickness and angle-of-incidence were not strongly correlated.

Tilt position	Thickness Å	MSE	Nominal angle °	Angle fit °	Fit - nominal °
-0.250	36.66	2.74	69	69.98	0.98
			72	72.86	0.86
			75	75.67	0.67
-0.125	37.72	2.35	69	69.73	0.73
			72	72.61	0.61
			75	75.43	0.43
0	38.83	2.30	69	69.48	0.48
			72	72.40	0.40
			75	75.22	0.22
0.125	38.69	2.33	69	69.33	0.33
			72	72.21	0.21
			75	75.03	0.03
0.250	*37.08*	*2.26*	*69*	*69.17*	*0.17*
			72	*72.03*	*0.03*
			75	*74.84*	*-0.16*
0.375	35.90	2.69	69	68.98	-0.02
			72	71.82	-0.18
			75	74.60	-0.40
0.500	34.29	2.58	69	68.84	-0.16
			72	71.66	-0.34
			75	74.44	-0.56

Table 10-3. Calculation of oxide thickness and angle of incidence for differing 'tilt' of the artefact

Graph 10-1 displays the deviation of the fitted angle from its corresponding nominal value. This clearly demonstrates the ability of the software to be able to sensibly model deviations of angle-of-incidence. The linearity of the results reflect that the levelling screw produces a uniform change in the angle-of-incidence over the tested range.

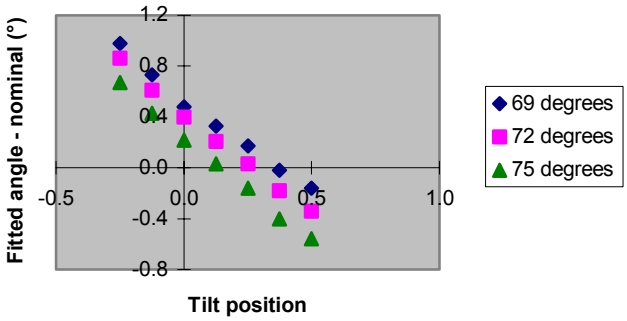

Graph 10-1. Deviation of fitted angle from nominal with respect to the 'tilt' of the artefact

However, as seen in Table 10-3, there also appears to be a systematic error in estimating the thickness that correlates with the deviation of the angle-of-incidence from its nominal value. This is displayed in Graph 10-2 and Graph 10-3; in the latter case the comparison has been made using the data measured at the nominal angle-of-incidence of 72°. The highlighted data (pointing arrow) in these graphs, and in Table 10-4 (*italics*), again correspond to the thickness determined at the 'zero point'. A reasonable assumption is that the thickness obtained when the nominal and the 'fit' values of angle agree, most accurately indicates oxide thickness. Graph 10-2 shows the trend is non-linear for extreme deviations of angle-of-incidence from nominal. A similar trend was established in a separate experiment when the tilt position was increased.

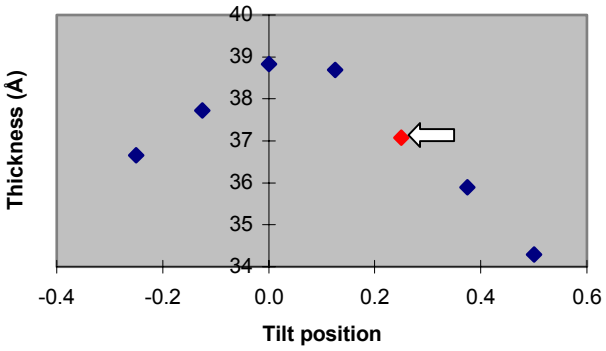

Graph 10-2: Oxide thickness as a function of tilt position

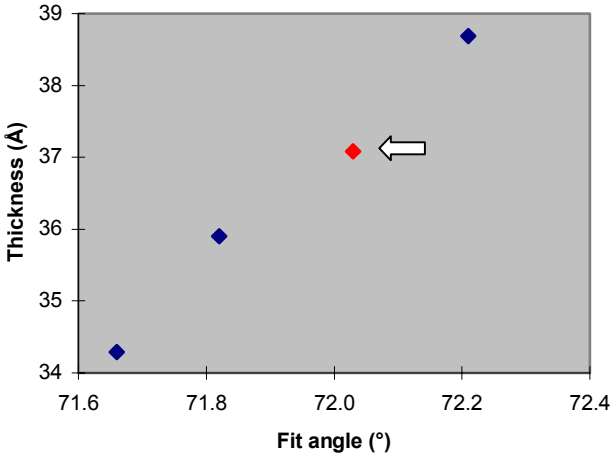

Graph 10-3: Oxide thickness as a function of angle of incidence

Graph 10-3 displays the thickness as a function of angle-of-incidence over the range of interest. A regression analysis revealed the slope of this graph to be 7.7Å per degree. A correction based on this value may be applied to the calculated thickness to take into account deviations of angle-of-incidence. Table 10-4 displays the results of this correction. One can see that the range and standard deviation of the corrected oxide thicknesses is significantly reduced.

Fit angle °	Difference °	Thickness Å	Corrected
72.21	0.21	38.69	37.07
72.03	*0.03*	*37.08*	*36.85*
71.82	-0.18	35.90	37.28
71.66	-0.34	34.29	36.91
	Mean	36.49	37.03
	Std dev.	1.86	0.20

Table 10-4: Corrected oxide thickness

10.6 Conclusions and future work

A procedure for using the focusing probes for the measurement of oxide thickness on flat and curved surfaces has been established. The main findings of this work can be summarised as:

- The angular spread for our system has been determined to be 2.2°.

- Due to a misalignment of the focusing lens(es), and possible errors associated with aligning a sample, the angle-of-incidence should be included in the fit parameters, especially for curved surfaces.

- A correction to the oxide thickness may need to be applied based on the deviation of the angle-of-incidence from nominal. The coefficient of this correction was measured as 7.7 Å per degree.

In the Avogadro project, the oxide thickness will ultimately have to be measured with an uncertainty of a few Ångstroms. When considering just the use and effective modelling of the focusing probes, errors of this magnitude may be easily introduced. Furthermore, when determining the above procedure, several assumptions were made to explain the results. It is vital that a complementary technique(s) is used to improve confidence in this approach. The measurements should also be repeated to establish the long term reproducibility of the set up.

The next stage of this work will be to determine the oxide thickness for a spherical artefact with a nominal diameter of 90 mm. Although its radius of curvature is less than that of the cylinder tested here, the alignment procedure could prove interesting!

11 APPENDIX 3: CALCULATION OF FILM THICKNESS USING XPS

There are three methods by which the thickness of a film on a substrate may be calculated [17]. The simplest method is to measure the intensity of the peak originating from the film I_f, which will increase with film thickness according to the relationship:

Equation 11–1

$$I_{f,d} = I_{f,\infty}(1 - e^{-d/(\lambda_f \sin\theta)})$$

where $I_{f,d}$ is the intensity of the peak corresponding to a film of thickness d, $I_{f,\infty}$ is the intensity from an infinitely thick film, λ_f is the attenuation length and θ is the take-off angle.

In a Si/SiO_2 system there are two choices for the oxide film peak: 1) electrons originating from the 1s level in the oxygen atoms (the O 1s peak); and 2) electrons originating from the 2p level of silicon atoms in the oxide (the Si 2p level). The later possibility exists because of the clear separation in the binding energies between the Si 2p substrate and oxide peaks. Due to inelastic scattering processes, an electron will not be able to escape from a film with a thickness of more than 15 nm or so, and no peak will be observed from the substrate. In this work, the intensity from an 'infinitely thick' oxide film was measured for a wafer, with a (100) orientation, which was subjected to an RCA clean followed by the growth of a thermal oxide with a thickness of approximately 17 nm. The intensity corresponding to an infinitely thick carbonaceous film was measured from a specimen of HDPE with a thickness of a few mm's. Immediately prior to measurement, a scalpel blade was used to rough the surface of this specimen, to remove any contaminants on its surface.

Conversely, one can measure the intensity of the Si 2p peak origination from the silicon substrate which will decrease exponentially with an increasing overlying film thickness:

Equation 11–2

$$I_{s,d} = I_{s,o} e^{-d/(\lambda_f \sin\theta)}$$

where $I_{s,d}$ is the intensity of the substrate peak from a sample covered with a film of thickness *d,* and $I_{s,0}$ is the peak from an oxide-free substrate.

$I_{s,0}$ has been obtained from a sample that, in-situ, was sputtered to remove the oxide layer.

Both methods rely on the characterisation of two different samples to determine a film's thickness. This has two disadvantages:

1. Reproducible analysis conditions are required;
2. The data may require a sizeable correction for any over-layer of adventitious carbon, which may differ for each sample.

The best solution is to base the analysis on the ratio of the Si 2p peaks from the substrate and oxide. In this case, the thickness is calculated using:

Equation 11–3

$$d=\lambda_f \sin\theta \ln(1+1/Q)$$

and Q is given by

Equation 11–4

$$Q=(I_{s,d}/I_{f,d})\,(I_{f,\infty}/I_{s,0})$$